Extracting Interpretable Models from Tree Ensembles: Computational and Statistical Perspectives

Brian Liu MIT Rahul Mazumder MIT Peter Radchenko University of Sydney

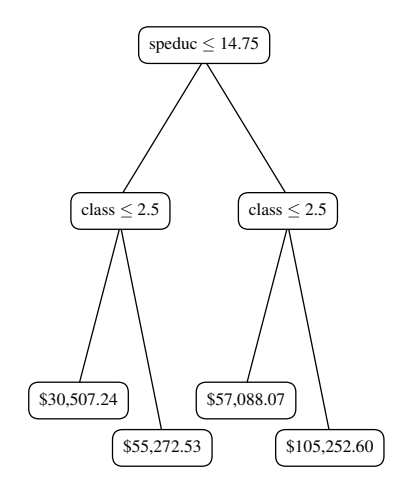
Abstract

Tree ensembles are non-parametric methods widely recognized for their accuracy and ability to capture complex interactions. While these models excel at prediction, they are difficult to interpret and may fail to uncover useful relationships in the data. We propose an estimator to extract compact sets of decision rules from tree ensembles. The extracted models are accurate and can be manually examined to reveal relationships between the predictors and the response. A key novelty of our estimator is the flexibility to jointly control the number of rules extracted and the interaction depth of each rule, which improves accuracy. We develop a tailored exact algorithm to efficiently solve optimization problems underlying our estimator and an approximate algorithm for computing regularization paths — sequences of solutions that correspond to varying model sizes. We also establish novel non-asymptotic prediction error bounds for our proposed approach, comparing it to an oracle that chooses the best data-dependent linear combination of the rules in the ensemble subject to the same complexity constraint as our estimator. The bounds illustrate that the large-sample predictive performance of our estimator is on par with that of the oracle. Through experiments, we demonstrate that our estimator outperforms existing algorithms for rule extraction.

Keywords: Interpretable Machine Learning, Tree Ensembles, Nonparametric Methods

1 Introduction

Tree ensemble algorithms, such as random forests (Breiman, 2001a) and gradient boosting (Friedman, 2002), are among the most well-known methods in statistical modeling and have achieved success across a broad range of disciplines, from remote sensing (Belgiu and Drăgut, 2016) to genomics (Chen and Ishwaran, 2012). Since their introduction, tree ensembles have earned a reputation for excellent predictive performance, in fact, Leo Breiman notably claims in *Statistical Modeling: The Two Cultures* (Breiman, 2001b) that "Random Forests are A+ predictors." By combining a large number of decision trees, either independently trained on bootstrapped samples of the data or sequentially on the residuals of the prior model, tree ensembles attain high predictive accuracy, albeit for an increase in model complexity and often at the expense of interpretability. Compared to a single tree, ensembles are substantially more challenging to interpret and, indeed, for random forests, Breiman (Breiman, 2001b, p. 208) claims that "on interpretability, they rate an F."



Model Explanation

- If speduc ≤ 14.75 and class ≤ 2.5 , then predicted income = \$30,507.24.
- If speduc ≤ 14.75 and class > 2.5, then predicted income = \$55,272.53.
- If speduc > 14.75 and class ≤ 2.5 , then predicted income = \$57,088.07.
- If speduc > 14.75 and class > 2.5, then predicted income = \$105,252.60.

Figure 1: Decision tree fit to predict household income using survey responses. Feature speduc is the spouse's education (years); class is the self-identified income class.

Consider, for example, the single decision tree shown in the left panel of Figure 1, constructed to predict household income based on survey responses from the 2022 General Social Survey (GSS) (Davern et al., 2024)—a dataset with 4,000 respondents and 15,000

covariates. This tree is highly interpretable, and its predictions can be fully explained in four sentences corresponding to the four rules listed in the right panel of the figure. Each rule consists of a sequence of conditions obtained by traversing the tree from the root node to a leaf. Tree ensembles can also be described by similar sets of rules, but these are rarely human-interpretable for two reasons. First, the number of rules is prohibitively large; for example, a boosting ensemble of 500 depth 6 trees requires 32,000 rules (sentences) to explain. Second, especially in deeper ensembles, each individual rule may be too complex to interpret. As Breiman (Breiman, 2001b, p. 208) observes for random forests:

"their mechanism for producing a prediction is difficult to understand. Trying to delve into the tangled web that generated a plurality vote from 100 trees is a Herculean task."

Yet, ensembles are significantly more accurate than single trees. On the GSS survey example, the decision tree shown in Figure 1 achieves an out-of-sample R^2 of **0.28** while the 500 depth 6 tree boosting ensemble mentioned above attains an out-of-sample R^2 of **0.55**.

Motivation:

"Framing the question as the choice between accuracy and interpretability is an incorrect interpretation of what the goal of statistical analysis is. The point of a model is to get useful information about the relation between the response and predictor variables." (Breiman, 2001b, p. 210)

To bridge the trade-off between model accuracy and interpretability, we propose a novel estimator to extract rule sets from tree ensembles. These rule sets retain predictive accuracy comparable to the full models, while being compact enough for practitioners to manually examine and understand the relationship between the predictors and the response. We consider compactness along two dimensions: the number of rules extracted (i.e., the number of sentences a practitioner must read to explain the model) and the interaction

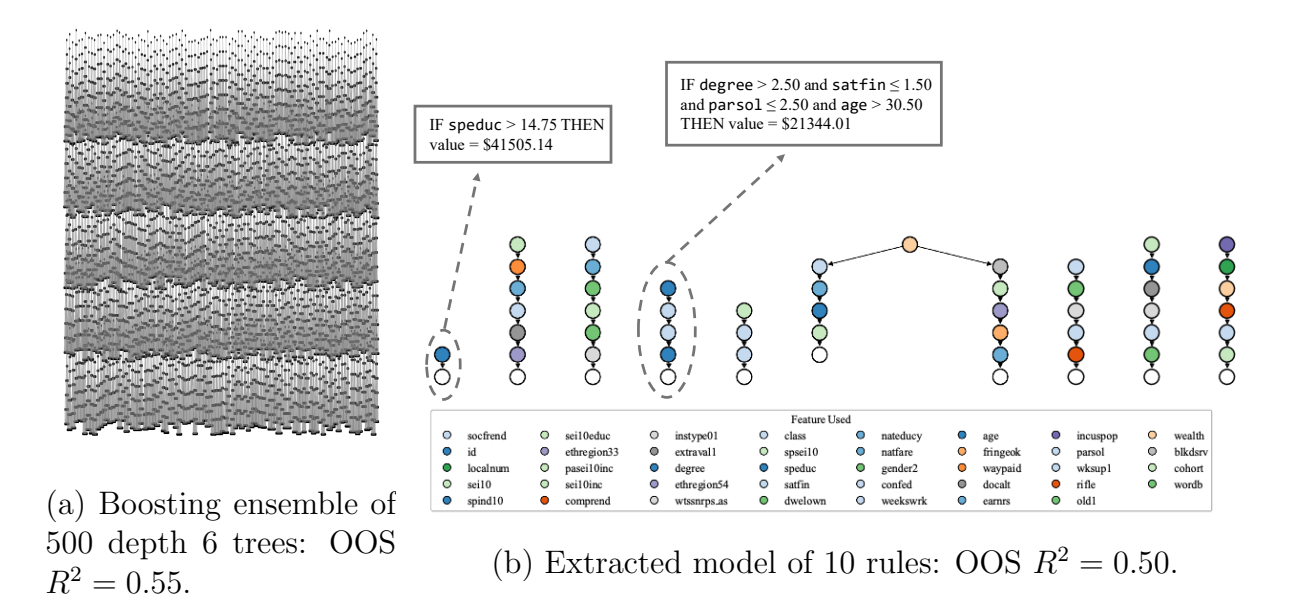


Figure 2: Application of our proposed estimator to the GSS example. Our estimator extracts a compact set of rules with varying interaction depths.

depth of each rule (i.e., the complexity of each sentence). In Figure 2, we demonstrate an application of our proposed estimator to the GSS example discussed above. Panel (a) visualizes the original boosting ensemble of 500 depth 6 trees (32,000 rules) that achieves an out-of-sample R^2 of 0.55. In panel (b), we apply our estimator to extract 10 rules from the ensemble, which achieve an out-of-sample R^2 of 0.50. Our estimator prunes the interaction depth of many rules and extracts a rule set compact enough to be examined by hand. Our proposed approach builds on prior work by Friedman and Popescu (2008), who use the LASSO to prune rules from random forests, and by Meinshausen (2010), who applies the non-negative garrote for rule extraction. Compared to existing methods, a key novelty of our estimator is its ability to jointly control both the number and depths of the extracted rules, a flexibility that leads to substantial improvements in predictive performance. In addition, to the best of our knowledge, we are the first to establish prediction error bounds for pruning rules from tree ensembles. We summarize our main contributions.

• We propose a novel estimator that uses an optimization-based framework to extract interpretable models from tree ensembles, offering the flexibility to jointly control both

the number of rules extracted and their interaction depths (§2).

- Our estimator is given by a discrete optimization problem that is difficult to solve due to its non-convexity. We develop a novel, specialized exact algorithm that solves this problem to global optimality and scales to sizes significantly beyond the capabilities of commercial solvers such as Gurobi (Gurobi Optimization, LLC, 2024) and Mosek (MOSEK ApS, 2024). With this exact algorithm, our estimator has theoretical guarantees (§3.1).
- We develop an approximate algorithm tailored for efficiently extracting sequences of models of varying sizes (i.e., regularization paths), allowing practitioners to assess the trade-off between model complexity and predictive accuracy. Although our estimator, when used with this algorithm, does not offer theoretical guarantees, the extracted rule sets are practically useful and exhibit strong empirical performance (§3.2).
- We establish non-asymptotic oracle prediction error bounds for our proposed approach.

 To the best of our knowledge, there are no other existing prediction error bounds for ensemble pruning algorithms (§4).
- We show through real world experiments that our estimator consistently outperforms state-of-the-art ensemble pruning algorithms at extracting interpretable rule sets (§5).

1.1 Preliminaries and Related Work

We first overview decision trees, rules, tree ensembles, and rule ensembles; we then discuss existing algorithms for extracting rules from tree ensembles (pruning) and highlight the advantages of our proposed estimator.

Decision Trees and Rules: We focus on regression trees for predicting a continuous response and use the terms regression tree and decision tree interchangeably throughout this paper. Regression trees consist of internal nodes and leaf nodes, where internal nodes represent splits that divide the data based on a selected feature and threshold. Splits are constructed greedily to grow the tree until a prespecified stopping criterion, such as the

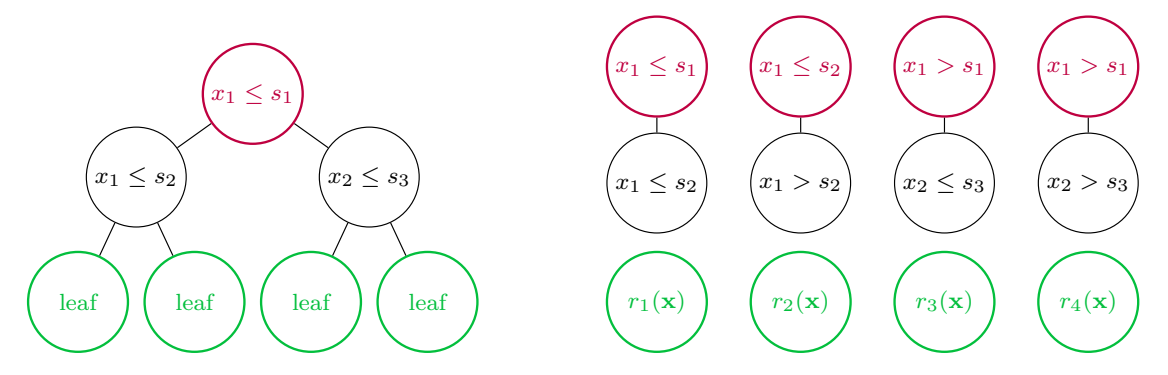


Figure 3: This tree has 4 leaf nodes and decomposes into 4 decision rules.

maximum depth of the tree, is reached. In the resulting leaf nodes, all observations in the node are assigned the same predicted value, the average response. Trees can be decomposed into sets of decision rules, where rules are defined by the sequences of splits obtained by traversing the tree from the root to leaves. We show an example in Figure 3; in the left panel we show a tree of depth 2, $\Gamma(\mathbf{x})$, which is a function of the feature vector $\mathbf{x} = (x_1, x_2)^{\mathsf{T}}$. This tree has 3 internal nodes and 4 leaf nodes, and values s_1 , s_2 , and s_3 represent split thresholds. In the right panel, we decompose the decision tree into 4 decision rules. Each rule is obtained by traversing the tree from root node (purple) to leaf node (green). For example, the prediction function for rule 2 is given by $r_2(\mathbf{x}) = \mathbbm{1}(x_1 \leq s_1) \cdot \mathbbm{1}(x_1 > s_2) \cdot \mu_2$, where μ_2 is the mean response of all of the observations in rule 2. We also have that $\Gamma(\mathbf{x}) = \sum_{j=1}^4 r_j(\mathbf{x})$ an important property that we leverage in our proposed estimator.

Tree Ensembles: Tree ensembles improve predictive performance by combining multiple decision trees. Popular approaches include bagging (e.g. random forests and adaptive bagging), which averages independently trained decision trees and boosting, which constructs a sequence of trees where each tree is fit on the residuals of the prior model. The resulting ensembles are powerful and have been shown to consistently outperform deep learning algorithms on tabular datasets (Shwartz-Ziv and Armon, 2022). However, with this increase in predictive performance comes a corresponding increase in model size and complexity. Tree ensembles can grow to be extremely large and, as such, these ensembles can be unwieldy,

slow at inference, and difficult to interpret due to their complexity.

Pruning: Tree ensembles can be pruned to improve model compactness and interpretability. One of the earliest computational approaches, ISLE, uses the LASSO to extract entire decision trees from an ensemble (Friedman et al., 2003). Subsequently, RuleFit (Friedman and Popescu, 2008) decomposes a tree ensemble into a large collection of decision rules and uses the LASSO to select a sparse subset. A closely related algorithm, Node Harvest (Meinshausen, 2010), applies the non-negative garrote to select a sparse subset of rules. Both RuleFit and Node Harvest become computationally expensive when the number of leaf nodes is large, which limits their application to smaller, shallower ensembles, typically of depth ≤ 3 . This limitation is restrictive, as deeper ensembles and rules may be needed to capture higher-order interactions in the data. More recently, FIRE (Liu and Mazumder, 2023a) uses techniques from non-convex optimization to improve the computational efficiency and predictive performance of rule extraction. Importantly, none of these methods are able to prune the depths of the extracted rules (see §A for additional discussion).

Interaction depth plays an important role in model complexity; in fact the depth of an ensemble, or its "interaction order is perhaps a more natural way to think of model complexity" (Efron and Hastie, 2021, Chapter 17) compared to other parameters such as the number of estimators. Extracting rules from deep ensembles without pruning their depth may not yield an interpretable model, as deep rules with long sequences of conditional statements can be difficult to understand. Conversely, a shallow rule set extracted from a shallow ensemble may lack the flexibility needed for strong predictive performance. Since existing rule extraction algorithms do not support depth pruning, they are unable to select rules of varying complexities. Recently, ForestPrune (Liu and Mazumder, 2023b), introduces an algorithm for pruning depth layers from tree ensembles. However, it is limited to pruning entire trees and does not support rule extraction. As a result, ForestPrune produces models that are less interpretable and less flexible than rule-based approaches.

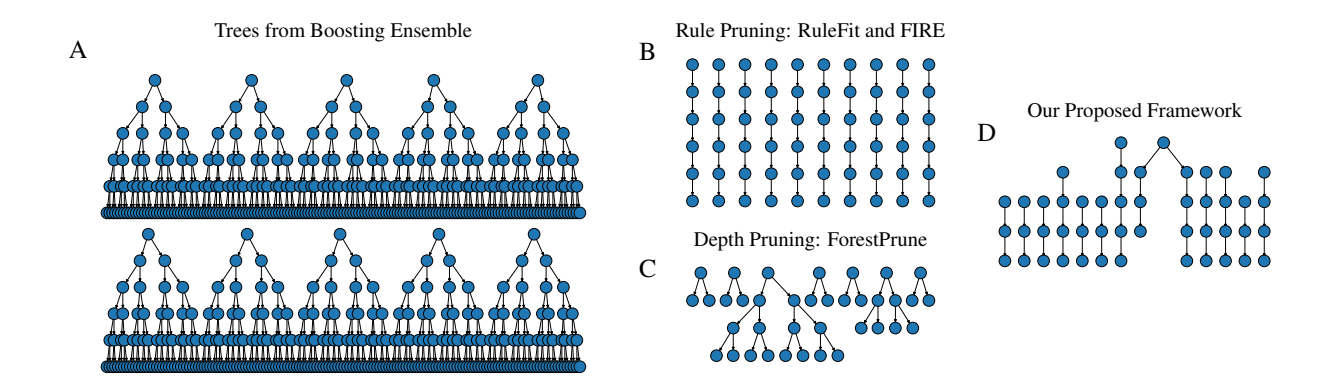


Figure 4: Visualization of our proposed framework, which jointly prunes depth and rules, compared with existing pruning approaches.

Our Proposed Approach: We propose a novel estimator that uses an optimization-based framework to simultaneously prune both rules and their interaction depths. Compared to existing approaches, our estimator is significantly more flexible and can extract rules with varying complexities. This allows us to prune and extract shallow rules for interpretability while retaining some deeper rules to capture higher-order interactions. The resulting rule sets achieve substantially higher predictive accuracy and improved interpretability compared to those extracted by existing methods.

We illustrate an application of our framework in comparison with existing methods in Figure 4. Specifically, we fit a boosting ensemble of 250 depth 5 decision trees on the WIND dataset from Haslett and Raftery (1989); a sample of 10 trees from the ensemble is displayed in panel A. In panel B, we illustrate the application of a rule pruning method such as RuleFit or FIRE. These methods extract rules without pruning depth, so all extracted rules retain the same depth as the original ensemble (depth 5). In panel C, we illustrate the application of ForestPrune. This method prunes entire trees but cannot extract individual rules, so the resulting model consists of a collection of pruned trees. Finally, in panel D, we illustrate the application of our framework, which jointly prunes both rules and interaction depth. This added flexibility improves the predictive performance of our estimator, compared to all existing methods, as demonstrated in §5.3. We also note that, in contrast to our method, none of the existing algorithms for pruning tree ensembles discussed above offer theoretical

guarantees. We formally present our estimator below.

2 Proposed Estimator

In this section, we present our estimator to jointly prune interaction depth and decision rules from a tree ensemble. Our estimator relies on the fact that we can represent the prediction of a tree ensemble as a linear combination of the extracted rules from each tree.

Notation: Given data matrix $X \in \mathbb{R}^{n \times p}$ and response $\mathbf{y} \in \mathbb{R}^n$, we fit a tree ensemble \mathcal{T} of T decision trees, $\{\Gamma_1(\mathbf{x}) \dots \Gamma_T(\mathbf{x})\}$, which are functions of the feature vector $\mathbf{x} \in \mathbb{R}^p$. Let m denote the total number of nodes in \mathcal{T} . Each decision tree $\Gamma_t(\mathbf{x})$, for all $t \in \mathcal{T}$ contains a set of \mathcal{N}_t nodes. This set includes both the leaf and the internal nodes. Each node $i \in \mathcal{N}_t$ has a pre-specified attribute a_i^t : this attribute can represent the depth of the node in the tree, the number of observations in the node, or some other prespecified characteristic. Also, for each node $i \in \mathcal{N}_t$ let \mathcal{C}_i^t represent the set of successor (descendant) nodes in tree $t \in \mathcal{T}$ and let \mathcal{P}_i^t represent the set of predecessor (parent) nodes. Finally, we use \mathbf{M}_i^t to represent the prediction vector for node i of tree t, for all $i \in \mathcal{N}_t$ and $t \in \mathcal{T}$. More specifically, we define vector $\mathbf{M}_i^t \in \mathbb{R}^n$ element-wise as follows: $(\mathbf{M}_i^t)_k = \mu_i^t \mathbbm{1}_{\{\text{node } i \text{ of tree } t \text{ contains obs. } k\}}$, where μ_i^t is the average response of all of the training observations in node i of tree t.

2.1 Formulation

We present the optimization-based formulation of our proposed estimator. For each node $i \in \mathcal{N}_t$, for all $t \in \mathcal{T}$, we introduce a binary decision variable $z_i^t \in \{0,1\}$ and a continuous decision variable $w_i^t \in \mathbb{R}$. A visualization of these decision variables for a single tree $t \in \mathcal{T}$ is shown in the left panel of Figure 5. The binary variable z_i^t indicates whether we select node $i \in \mathcal{N}_t$ as a terminal node for a rule in the pruned ensemble. If $z_i^t = 1$, we extract the corresponding rule by traversing tree t from the root to node i. For example, in the right

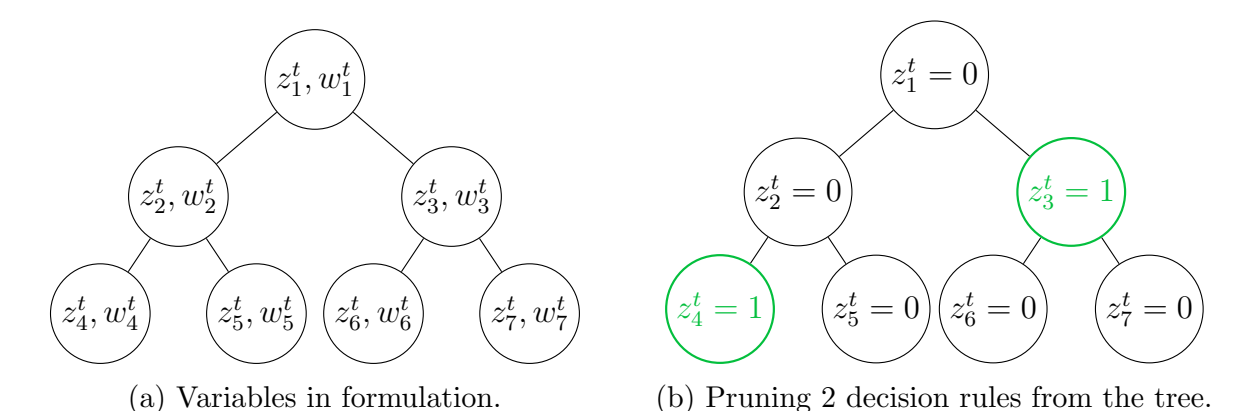


Figure 5: Each binary decision variable z_i^t indicates whether node i in tree t is selected to be a terminal node of a rule. Set C_i^t represents the set of descendant nodes for node i, for example, $C_3^t = \{6, 7\}$. If node 3 is selected to be a terminal node in an extracted rule then nodes 6 and 7 cannot be selected.

panel of Figure 5, setting $z_4^t = 1$ extracts the depth 2 rule obtained by traversing the tree from nodes 1 (root) to 2 to 4. Likewise, setting $z_3^t = 1$ extracts the depth 1 rule obtained by traversing the tree from nodes 1 (root) to 3. Continuous variable w_i^t specifies the weight assigned to each extracted rule, and the prediction of our pruned model is then given by the weighted sum of the rule predictions: $\sum_{t \in \mathcal{T}} \sum_{i \in \mathcal{N}_t} \mathbf{M}_i^t w_i^t$. We use the following problem to prune rules and interaction depth from tree ensembles.

$$\min_{z_i^t, w_i^t} \quad \frac{1}{2} \left\| \mathbf{y} - \sum_{t \in \mathcal{T}} \sum_{i \in \mathcal{N}_t} \mathbf{M}_i^t w_i^t \right\|_2^2 + \frac{1}{2\gamma} \sum_{t \in \mathcal{T}} \sum_{i \in \mathcal{N}_t} (w_i^t)^2$$
 (1)

s.t.
$$\sum_{j \in \mathcal{C}_i^t} z_j^t \leq |\mathcal{C}_i^t| z_i^t, \quad \forall \ i \in \mathcal{N}_t, \ t \in \mathcal{T},$$
 (Constraint 1a)

$$\sum_{t \in \mathcal{T}} \sum_{i \in \mathcal{N}_t} a_i^t z_i^t \le K,$$
 (Constraint 1b)

$$(1 - z_i^t) w_i^t = 0, \quad \forall \ i \in \mathcal{N}_t, \ t \in \mathcal{T},$$
 (Constraint 1c)

$$z_i^t \in \{0, 1\}, \quad \forall \ i \in \mathcal{N}_t, \ t \in \mathcal{T}.$$
 (Constraint 1d)

The first term in the objective of Problem (1) is the quadratic loss function, which captures data fidelity, and the second term is a ridge regularization penalty. We include this penalty mainly for computational reasons, however, we note that ridge regularization may improve

the predictive performance of our estimator in low signal-to-noise ratio regimes (Mazumder et al., 2023). Parameter K restricts the sum of attributes of the extracted rules and parameter γ controls the ridge penalty. We discuss the constraints of Problem (1) below.

Constraint (1a), Valid Rule Prunings: This constraint ensures that the rule prunings are valid for each tree. If node i in tree t is selected to be the terminal node of an extracted rule, none of its successor nodes, $j \in C_i^t$, can be selected to be terminal nodes.

Constraint (1b), Attribute-Weighted Budget: This constraint controls the sum of attributes of the rules extracted into the pruned model. For example, if we set attribute $a_i^t = 1$ for all $i \in \mathcal{N}_t$ and $t \in \mathcal{T}$, this constraint directly restricts the number of rules selected into the pruned model to be less than or equal to K. There are many interesting choices for attribute a_i^t , which is prespecified. For example, setting a_i^t to the depth of each node can result in shallower rule sets; we discuss various choices of a_i^t in §2.2.2.

Constraint (1c), Coupling: Finally, constraint (1c) couples binary variable z_i^t with variable w_i^t and constraint (1d) restricts variables z_i^t to be binary. This ensures that only extracted rules are assigned a non-zero weight.

Problem (1) is a mixed-integer program (MIP) with m binary decision variables and m continuous decision variables, where m is the total number of nodes in \mathcal{T} . We note that m is typically large. For instance, a boosting ensemble of 1000 depth 3 trees has $m \approx 10^4$; off-the-shelf optimization software such as Gurobi struggle to scale to these problem sizes. Consequently, we present a tailored exact algorithm (§3.1) to solve Problem (1) to optimality, that scales to problem sizes beyond the capabilities of commercial solvers.

2.2 Practical Considerations

We give further details on our estimator, discussing both regularization paths and how different choices of node attributes influence the extracted model.

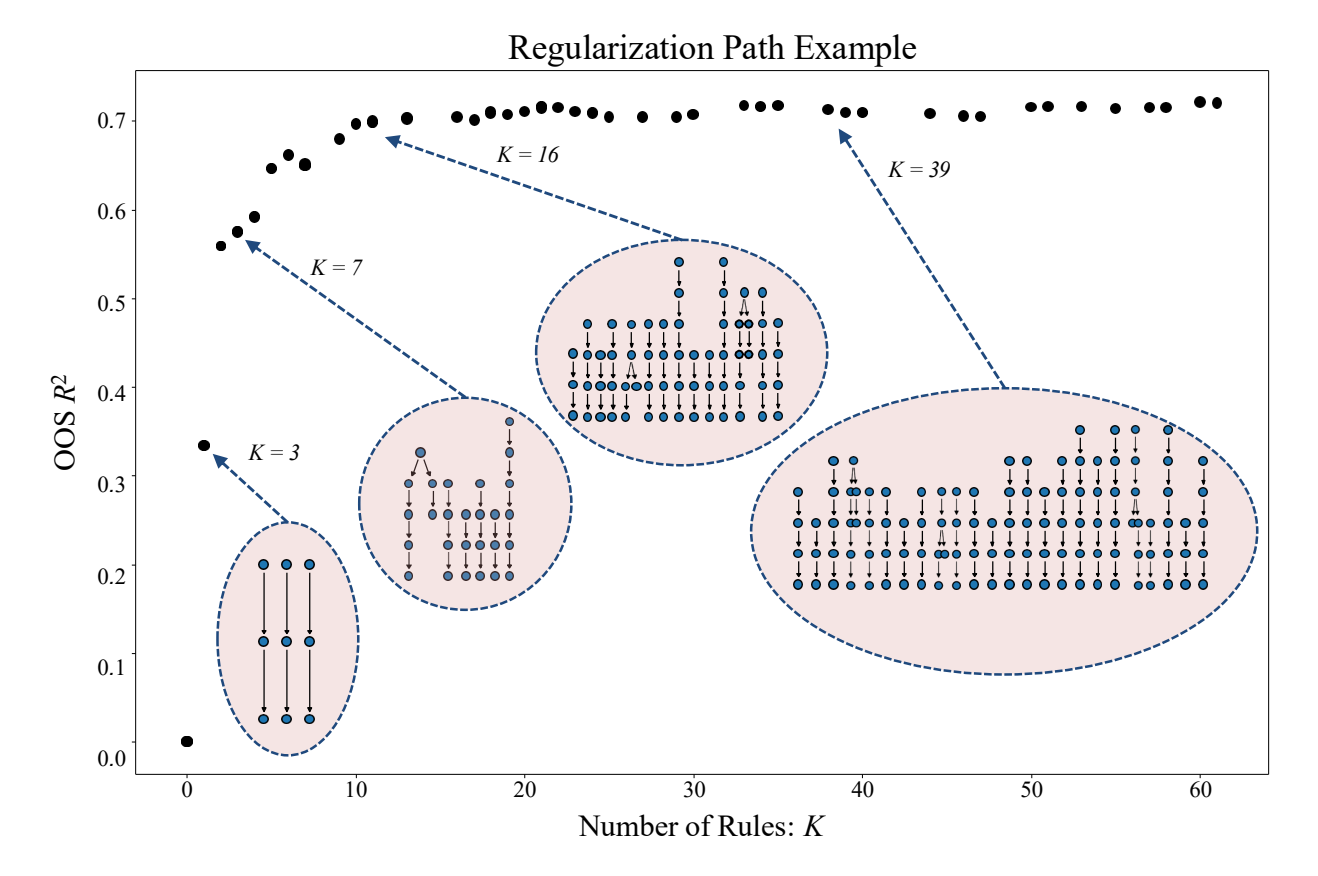


Figure 6: Example regularization path computed by our framework on the WIND example from Haslett and Raftery (1989). The path consists of a sequence of solutions that correspond to varying model sizes and predictive performances.

2.2.1 Regularization Paths

Solving Problem (1) within our optimization framework prunes an ensemble under a fixed budget K, which controls the number of rules extracted. The predictive accuracy of the extracted model can vary significantly with model size, and, in practice, appropriate values of K may not be known a priori. As such, we recommend finding solutions to Problem (1) across a range of K values to asses the tradeoff between model accuracy and size.

We refer to this process as computing the **regularization path** in our framework, that is, generating a sequence of solutions with varying model sizes, analogous to the regularization path in sparse regression. In Figure 6, we show an example of such a path, computed on an example where we prune a boosting ensemble of 500 depth 5 decision trees fit on the WIND dataset from Haslett and Raftery (1989). In this example, we set every

node attribute $a_i^t = 1$, $\forall i \in \mathcal{N}_t$, $t \in \mathcal{T}$, so that K directly controls the number of rules in the extracted model. The horizontal axis in Figure 6 shows K, the number of rules extracted, and the vertical axis shows the out-of-sample R^2 of the extracted model; each point in the scatter plot shows a solution obtained along the regularization path. The displays in the highlighted circles show snapshots of the extracted models with $K \in \{3, 7, 16, 39\}$ rules.

From this regularization path, we observe that the out-of-sample predictive accuracies of the extracted rules increase sharply with K up to K=16. Beyond this point, further increases in K lead to greater model complexity with minimal gains in accuracy. Computing regularization paths allows practitioners to explore the tradeoff between model size and predictive accuracy and select an appropriate model. A key component of our framework is an efficient procedure for computing regularization paths, which we present in §3.2.

2.2.2 Node Attributes

Here, we discuss choices for node attributes a_i^t , $\forall i \in \mathcal{N}_t$, $t \in \mathcal{T}$ and their corresponding effects on the extracted models.

Rule-Weighting: In the rule-weighting scheme, we define $a_i^t = 1$ for all $i \in \mathcal{N}_t$, $t \in \mathcal{T}$. With this choice, the attribute-weighted budget constraint (1b) directly controls the number of rules to extract. This assignment provides the most straightforward interpretation of constraint (1b) and offers the most direct control over model size, so we use it as the default in our framework.

Depth-Weighting: In the depth-weighting scheme, we define $a_i^t = |\mathcal{P}_i^t|$ for all $i \in \mathcal{N}_t$, $t \in \mathcal{T}$, where $|\mathcal{P}_i^t|$ denotes the number of ancestor nodes of node i in tree t. This quantity corresponds to the interaction depth of node i—that is, the number of conditions traversed from the root to node i. Constraint (1b) budgets the sum of interaction depths in the extracted model, which encourages the extraction of shallower rules. This may improve model interpretability and compactness compared to rule-weighting.

Feature-Weighting: In the feature-weighting scheme, we set a_i^t equal to the number of distinct features that appear in \mathcal{P}_i^t for all $i \in \mathcal{N}_t$, $t \in \mathcal{T}$, i.e., the number of distinct features that appear in the ancestor nodes of node i in tree t. This is the number of feature interactions required to reach node i from the root node. As a result, constraint (1b) better controls the feature interaction depth and overall feature sparsity of the extracted model.

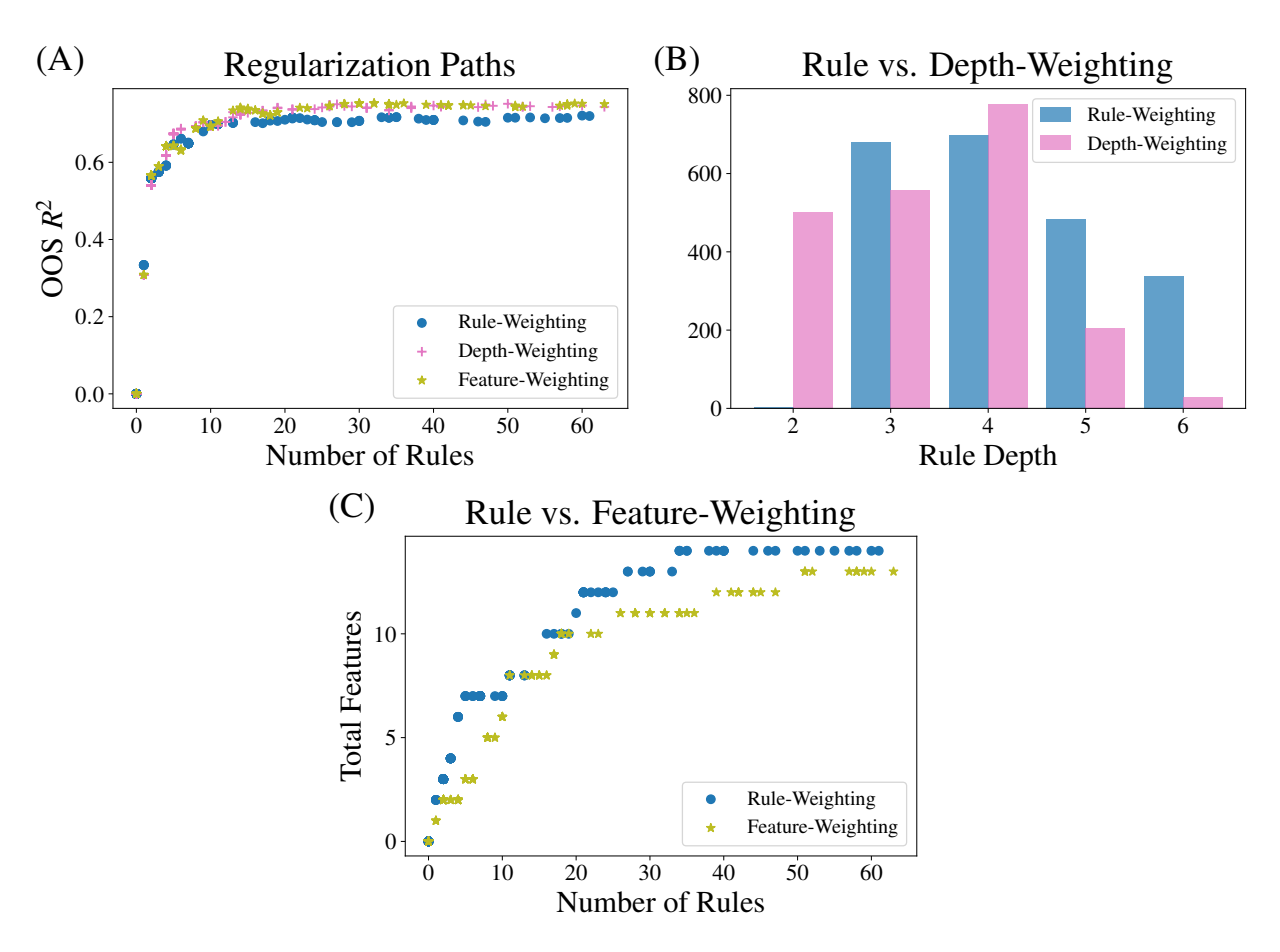


Figure 7: Comparison of the effects of different node attributes on the extracted models. Compared to rule-weighting, depth-weighting extracts shallower rules and feature-weighting promotes feature sparsity.

Comparison of Attribute Weighting Schemes: In Figure 7, we compare the effects of rule-weighting, depth-weighting, and feature-weighting on the models extracted by our estimator. We prune the same boosted ensemble from above, of 500 depth 5 trees fit on the WIND dataset (Haslett and Raftery, 1989), and compute regularization paths under each of the three weighting schemes. Panel A of Figure 7 displays these paths, where the horizontal

axis denotes model size (in number of rules) and the vertical axis shows the out-of-sample \mathbb{R}^2 . While all three schemes yield similar predictive performances, the extracted models exhibit markedly different structural properties. In panel B, we compare the distribution of rule-depths between the models extracted by depth-weighting and rule-weighting, across the entire regularization path. From this plot, it is apparent that depth-weighting extracts shallower rules. In panel C, we compare the total number of features used in the models extracted by feature-weighting and rule-weighting. From this plot, we see that feature-weighting promotes greater feature sparsity across the regularization path.

3 Optimization Algorithms

In this section, we present our optimal algorithm (§3.1) to solve instances of Problem (1) as well as our approximate algorithm (§3.2) to efficiently compute regularization paths. Empirically, we observe that solutions obtained by our optimal algorithm perform better in terms of out-of-sample performance compared to those obtained by our approximate algorithm, and, in addition, have theoretical guarantees. Our approximate algorithm, however, scales to larger problem sizes and can efficiently compute solution paths across varying levels of sparsity. While lacking in terms of theoretical guarantees, we observe that the solutions obtained by our approximate algorithm are practically useful.

3.1 Optimal Algorithm

We present here a tailored exact algorithm¹ to solve instances of Problem (1) to global optimality. Our algorithm can scale to problem sizes beyond the capabilities of off-the-shelf optimization solvers, such as MOSEK and Gurobi, and can solve instances of Problem (1) with thousands of observations and decision variables in seconds. To achieve this speedup, we reformulate Problem (1) as a convex integer program (CIP) that depends only on binary

 $^{^{1}\}mathrm{We}$ use the terms exact algorithm and optimal algorithm interchangeably.

decision variables \mathbf{z} , halving the number of decision variables. We develop a tailored outer approximation algorithm which exploits problem sparsity and the convexity of the objective function to solve the reformulation to optimality.

Problem Reformulation: Let $\mathbf{z} \in \{0, 1\}^m$ denote the vector containing decision variables z_i^t for all $i \in \mathcal{N}_t$ and $t \in \mathcal{T}$; recall that tree ensemble \mathcal{T} contains $m = \sum_{t \in \mathcal{T}} |\mathcal{N}_t|$ nodes. Let \mathbb{I}_n denote the n-dimensional identity matrix and consider the integer program

$$\min_{\mathbf{z}} \quad q(\mathbf{z}) = \frac{1}{2} \mathbf{y}^{\top} \left(\mathbb{I}_n + \gamma \sum_{t \in \mathcal{T}} \sum_{i \in \mathcal{N}_t} z_i^t \mathbf{M}_i^t (\mathbf{M}_i^t)^{\top} \right)^{-1} \mathbf{y}$$
 (2)

s.t.
$$\sum_{j \in \mathcal{C}_i^t} z_j^t \leq |\mathcal{C}_i^t| z_i^t, \quad \forall \ i \in \mathcal{N}_t, \ t \in \mathcal{T},$$
 (Constraint 2a)

$$\sum_{t \in \mathcal{T}} \sum_{i \in \mathcal{N}_t} a_i^t z_i^t \le K,$$
 (Constraint 2b)

$$z_i^t \in \{0, 1\}, \quad \forall \ i \in \mathcal{N}_t, \ t \in \mathcal{T}.$$
 (Constraint 2c)

The propositions below state some properties of Problem (2).

Proposition 1. Problem (2) is an equivalent reformulation of Problem (1).

Proposition 2. Objective $\mathbf{z} \mapsto q(\mathbf{z})$ where $q(\mathbf{z})$ is defined in (2) is convex on $\mathbf{z} \in [0,1]^m$.

We prove these propositions in §B.1 of the appendix. Problem (2) is a convex integer program with m binary decision variables and linear constraints (2a) and (2b). We say that $\mathbf{z} \in \mathbb{C}_3$ if decision vector \mathbf{z} satisfies the 3 constraints in $\mathbb{C}_3 = \{(2a), (2b), (2c)\}$

Outer Approximation Algorithm: We present a specialized outer approximation (OA) algorithm to solve Problem (2) to optimality (Bertsimas and Van Parys, 2020; Duran and Grossmann, 1986). We treat Problem (2) as an *implicit* reformulation; our outer approximation algorithm only needs to evaluate the objective $q(\mathbf{z})$ and its subgradient $\nabla q(\mathbf{z})$. Because Constraint (2b) typically yields a sparse \mathbf{z} , we can perform these evaluations efficiently without explicitly constructing Problem (2)—see Appendix §B.2 for details.

Objective function $q(\mathbf{z})$ in Problem (2) is convex, so for all $\mathbf{z}' \in [0, 1]^m$ we have: $q(\mathbf{z}') \geq q(\mathbf{z}) + \nabla q(\mathbf{z})^{\top}(\mathbf{z}' - \mathbf{z})$. Given a sequence of feasible solutions $\mathbf{z}^{(\mathbf{0})}, \mathbf{z}^{(\mathbf{1})}, \dots \mathbf{z}^{(\mathbf{h})}$ for Problem (2), we have that: $Q_{LB,h}(\mathbf{z}) := \max_{k=0,\dots,h} q(\mathbf{z}^{(\mathbf{k})}) + \nabla q(\mathbf{z}^{(\mathbf{k})})(\mathbf{z} - \mathbf{z}^{(\mathbf{k})}) \leq q(\mathbf{z})$, where function $\mathbf{z} \mapsto Q_{LB,h}(\mathbf{z})$ is a piecewise linear lower bound on function $\mathbf{z} \mapsto q(\mathbf{z})$. In each iteration h of our outer approximation algorithm, we minimize $Q_{LB,h}(\mathbf{z})$ with respect to $\mathbf{z} \in \mathbb{C}_3$ to obtain $\mathbf{z}^{(\mathbf{h}+\mathbf{1})}$ by solving the problem:

$$\min_{\mathbf{z},\nu} \quad \nu \quad \text{s.t.} \quad \mathbf{z} \in \mathbb{C}_3, \quad \nu \ge q(\mathbf{z}^{(\mathbf{k})}) + \nabla q(\mathbf{z}^{(\mathbf{k})})(\mathbf{z} - \mathbf{z}^{(\mathbf{k})}) \quad \forall \ k \in \{0, 1, \dots, h\}, \quad (3)$$

where ν is a lower bound for the optimal objective value $q(\mathbf{z}^*)$. We present our full outer approximation algorithm in Algorithm 1.

```
Algorithm 1: Outer Approximation Algorithm for Problem (2)
```

```
1 \mathbf{z^{(0)}} \leftarrow \text{warm start}, \ \nu^{(0)} \leftarrow q(\mathbf{z^{(0)}}), \ h \leftarrow 0
2 \mathbf{while} \ q(\mathbf{z^{(h)}}) > \nu^{(h)} \ \mathbf{do}
3 | add cutting plane \nu^{(h)} \geq q(\mathbf{z^{(h)}}) + \nabla q(\mathbf{z^{(h)}})(\mathbf{z} - \mathbf{z^{(h)}}) \text{ to Problem (3)}
4 | solve Problem (3) for \mathbf{z^{(h+1)}}
5 | \mathbf{h} = \mathbf{h} + 1
6 \mathbf{end}
7 \mathbf{return} \ \mathbf{z^*}
```

We terminate our algorithm when our objective value $q(\mathbf{z}^{(\mathbf{h})})$ is equal to the lower bound for the optimal objective value, $\nu^{(h)}$. Since the number of feasible solution in \mathbb{C}_3 is finite, Algorithm 1 terminates in a finite number of iterations (Fletcher and Leyffer, 1994) and returns the optimal solution \mathbf{z}^* to Problem (2). Let S^* represent the set of nonzero indices of \mathbf{z}^* , i.e., $S^* = \{i : z_i^* \neq 0\}$, and let \mathcal{M} be the matrix formed by taking the vectors \mathbf{M}_i^t as columns for all $i \in \mathcal{N}_t$ and $t \in \mathcal{T}$. Let \mathcal{M}_{S^*} be the sub-matrix of \mathcal{M} formed by selecting the columns corresponding to S^* . We have that $\mathbf{w}^* = \left(\frac{\mathbb{I}_{|S^*|}}{\gamma} + (\mathcal{M}_{S^*}^t)^\top \mathcal{M}_{S^*}\right)^{-1} \mathcal{M}_{S^*} y$, and that \mathbf{w}^* , \mathbf{z}^* is the optimal solution to Problem (1). In each iteration of Algorithm 1 we must solve Problem (3), an integer linear program with m binary decision variables. This can be done efficiently in seconds using off-the-shelf solvers, for values up to $m \approx 10^5$. Our tailored exact algorithm solves Problem (1) to optimality over three orders of magnitude faster than commercial solvers. For example, consider a boosting ensemble of 100 depth 3 decision trees, fit on the SOCMOB social mobility dataset from Biblarz and Raftery (1993). This dataset contains around 1000 observations and the resulting ensemble contains $m \approx 1500$ nodes. We want to use our estimator to extract a compact rule set of 20 rules. Algorithm 1 can solve Problem (1) to optimality in under **2 seconds**, while Gurobi fails to find the optimal solution in **3 hours**. In §5.1, we evaluate the computation time of our exact algorithm compared to commercial solvers across a range of problem sizes.

3.2 Approximate Algorithm

We introduce an approximate algorithm that efficiently finds high-quality solutions to Problem (1) and is tailored for computing regularization paths. Motivated by the success of approximate algorithms for penalized formulations of high-dimensional sparse regression (Hazimeh et al., 2023), we consider this penalized reformulation of Problem (1):

$$\min_{z_i^t, w_i^t} \frac{1}{2} \left\| \mathbf{y} - \sum_{t \in \mathcal{T}} \sum_{i \in \mathcal{N}_t} \mathbf{M}_i^t w_i^t \right\|_2^2 + \frac{1}{2\gamma} \sum_{t \in \mathcal{T}} \sum_{i \in \mathcal{N}_t} (w_i^t)^2 + \lambda \sum_{t \in \mathcal{T}} \sum_{i \in \mathcal{N}_t} a_i^t z_i^t \qquad (4)$$
s.t.
$$\sum_{j \in \mathcal{C}_i^t} z_j^t \leq |\mathcal{C}_i^t| z_i^t, \quad (1 - z_i^t) w_i^t = 0, \quad z_i^t \in \{0, 1\}, \quad \forall i \in \mathcal{N}_t, \ t \in \mathcal{T},$$

where parameter λ controls the size of the extracted model. Our approximate algorithm finds solutions to Problem (4) across a range of λ values to compute regularization paths. As an aside, in D of the appendix we explore the convex relaxation of Problem (4) as a new estimator of independent interest.

Note that the first term in the objective function of Problem (4) is smooth with respect to w, the second and third terms are separable with respect to trees $t \in \mathcal{T}$. The constraints are also all separable with respect to trees $t \in \mathcal{T}$. We apply the following block coordinate descent (BCD) algorithm to find high-quality solutions to Problem (4). For a fixed block

 $t \in \mathcal{T}$, let δ represent the remaining blocks, i.e., $\delta = \mathcal{T} \setminus t$, and let residual vector $\mathbf{r} = \mathbf{y} - \sum_{t \in \delta} \sum_{i \in \mathcal{N}_t} \mathbf{M}_i^t w_i^t$. Each update of our BCD algorithm solves the MIP:

$$\min_{\mathbf{z}^{t}, \mathbf{w}^{t}} \quad \frac{1}{2} \left\| \mathbf{r} - \sum_{i \in \mathcal{N}_{t}} \mathbf{M}_{i}^{t} w_{i}^{t} \right\|_{2}^{2} + \frac{1}{2\gamma} \sum_{i \in \mathcal{N}_{t}} (w_{i}^{t})^{2} + \lambda \sum_{i \in \mathcal{N}_{t}} a_{i}^{t} z_{i}^{t}$$
s.t.
$$\sum_{j \in \mathcal{C}_{i}^{t}} z_{j}^{t} \leq |\mathcal{C}_{i}^{t}| z_{i}^{t}, \quad (1 - z_{i}^{t}) w_{i}^{t} = 0, \quad z_{i}^{t} \in \{0, 1\}, \quad \forall i \in \mathcal{N}_{t},$$

where the decision vectors $\mathbf{z}^{\mathbf{t}} \in \{0,1\}^{|\mathcal{N}_t|}$ and $\mathbf{w}^{\mathbf{t}} \in \mathbb{R}^{|\mathcal{N}_t|}$ represent the stacked decision variables z_i^t and w_i^t for all $i \in \mathcal{N}_t$, i.e., the decision variables associated with tree $t \in \mathcal{T}$.

```
Algorithm 2: Cyclic Block Coordinate Descent for Problem (4)
```

```
1 \mathbf{z}, \mathbf{w} \leftarrow \text{warm start}
2 \mathbf{repeat}
3 | \mathbf{for} \ t \in \mathcal{T} \ \mathbf{do}
4 | \mathbf{solve} \ \text{MIP} \ (5) \ \text{for} \ z_i^t, \ w_i^t \ \forall i \in \mathcal{N}_t
5 | \mathbf{end}
6 \mathbf{until} \ until \ objective \ no \ longer \ improves;
7 \mathbf{return} \ \mathbf{z}, \mathbf{w}
```

We summarize our proposed cyclic BCD procedure in Algorithm 2. Algorithm 2 returns a sequence of non-increasing objective values for Problem (4), and we terminate our algorithm when the objective no longer improves. Our CBCD algorithm depends on our ability to solve Problem (5), a MIP with $|\mathcal{N}_t|$ binary and $|\mathcal{N}_t|$ continuous decision variables, efficiently. In the next section, we present a procedure to do so and introduce computational enhancements that allow Algorithm (2) to efficiently compute regularization paths.

3.2.1 Computational Enhancements

In §5.2, we evaluate the impact of the enhancements presented below on the computation time of our approximate algorithm,.

Efficient Block Update: We present an outer approximation procedure similar to the

one discussed in §3.1 to solve Problem (5) efficiently. Consider the following IP:

$$\min_{\mathbf{z}^{t}} \quad q_{\mathbf{r}}(\mathbf{z}^{t}) = \frac{1}{2} \mathbf{r}^{\mathsf{T}} \left(\mathbb{I}_{n} + \gamma \sum_{i \in \mathcal{N}_{t}} z_{i}^{t} \mathbf{M}_{i}^{t} (\mathbf{M}_{i}^{t})^{\mathsf{T}} \right)^{-1} \mathbf{r} + \lambda \sum_{i \in \mathcal{N}_{t}} a_{i}^{t} z_{i}^{t}$$
s.t.
$$\sum_{j \in \mathcal{C}_{i}^{t}} z_{j}^{t} \leq |\mathcal{C}_{i}^{t}| z_{i}^{t}, \quad z_{i}^{t} \in \{0, 1\}, \quad \forall i \in \mathcal{N}_{t}.$$

The following proposition establishes some properties of Problem (6).

Proposition 3. Problem (6) is an equivalent reformulation of MIP Problem (5) and objective function $\mathbf{z^t} \mapsto q_{\mathbf{r}}(\mathbf{z^t})$ is convex on $\mathbf{z^t} \in [0,1]^{|\mathcal{N}_t|}$.

We prove this proposition and present an efficient procedure to evaluate $q_{\mathbf{r}}(\mathbf{z}^{\mathbf{t}})$ and $\nabla q_{\mathbf{r}}(\mathbf{z}^{\mathbf{t}})$ in §C.1 of the appendix.

In each iteration h of our outer approximation algorithm we solve this ILP, using off-the-shelf solvers, to obtain $(\mathbf{z}^{\mathbf{t}})^{(h+1)}$:

$$\min_{\mathbf{z}^{t},\nu} \quad \nu \quad \text{s.t.} \quad \sum_{j \in \mathcal{C}_{i}^{t}} z_{j}^{t} \leq |\mathcal{C}_{i}^{t}| z_{i}^{t}, \quad z_{i}^{t} \in \{0,1\}, \quad \forall i \in \mathcal{N}_{t},$$

$$\nu \geq q_{\mathbf{r}} ((\mathbf{z}^{t})^{(\mathbf{k})}) + \nabla q_{\mathbf{r}} ((\mathbf{z}^{t})^{(\mathbf{k})}) (\mathbf{z} - (\mathbf{z}^{t})^{(\mathbf{k})}) \quad \forall k \in \{0,\dots,h\}.$$
(7)

```
Algorithm 3: Outer Approximation Algorithm for Problem (6)
```

```
1 (\mathbf{z^t})^{(0)} \leftarrow \text{warm start}, \ \nu^{(0)} \leftarrow q_{\mathbf{r}}((\mathbf{z^t})^{(0)}), \ h \leftarrow 0
2 while q_{\mathbf{r}}((\mathbf{z^t})^{(h)}) > \nu^{(h)} do
3 | add cutting plane \nu^{(h)} \geq q_{\mathbf{r}}((\mathbf{z^t})^{(h)}) + \nabla q_{\mathbf{r}}((\mathbf{z^t})^{(h)})(\mathbf{z} - (\mathbf{z^t})^{(h)}) to Problem (7)
4 | solve Problem (7) for (\mathbf{z^t})^{(h+1)}
5 | h = h+1
6 end
7 return (\mathbf{z^t})^*
```

We present our outer approximation procedure in Algorithm 3, which converges in a finite number of iterations (Fletcher and Leyffer, 1994) and returns the optimal solution $(\mathbf{z}^{\mathbf{t}})^*$ to Problem (6). Let S^* correspond to the set of indices where $(\mathbf{z}^{\mathbf{t}})^* \neq 0$, let \mathcal{M}^t

denote the $n \times |\mathcal{N}_t|$ matrix formed by taking vectors \mathbf{M}_i^t as columns for all $i \in \mathcal{N}_t$, and let $\mathcal{M}_{S^*}^t$ be the sub-matrix of \mathcal{M}^t formed by selecting the columns corresponding to indices in S^* . We have that $(\mathbf{w^t})^* = \left(\frac{\mathbb{I}_{|S^*|}}{\gamma} + (\mathcal{M}_{S^*}^t)^\top \mathcal{M}_{S^*}^t\right)^{-1} \mathcal{M}_{S^*}^t r$, and that $(\mathbf{w^t})^*$, $(\mathbf{z^t})^*$ is the optimal solution to Problem (5). Below, we present several enhancements to speed up our CBCD Algorithm 2, along with a procedure to efficiently compute regularization paths.

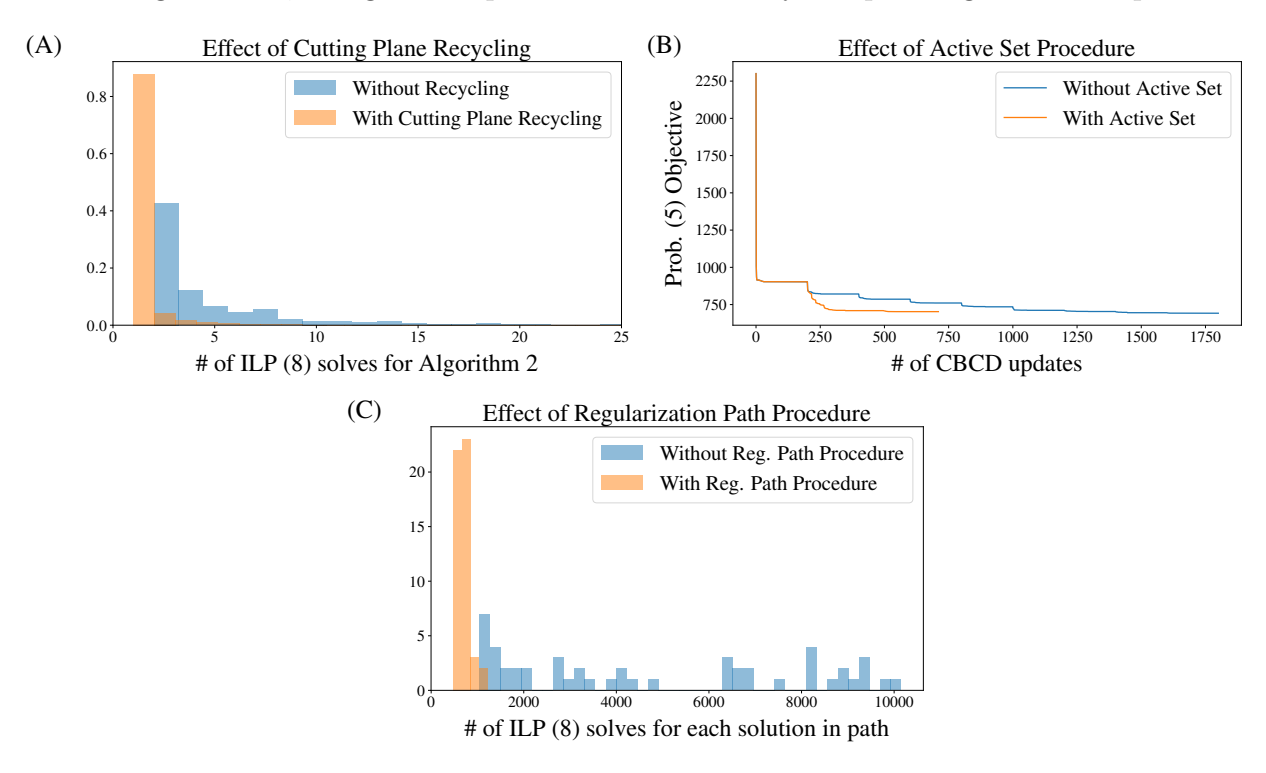


Figure 8: **Panel A:** Cutting plane recycling reduces the number of ILP solves required for Algorithm 3. **Panel B:** Active set optimization reduces the number of CBCD updates required in Algorithm 2. **Panel C:** Our efficient regularization path procedure reduces the number of ILP solves required for each solution in the path. These visualizations are from an application of our framework on the WIND dataset from Haslett and Raftery (1989).

Cutting Plane Recycling: In Algorithm 2 we update each block, tree $t \in \mathcal{T}$, multiple times. Only the residual vector \mathbf{r} changes between updates; the constraints in Problem (6) remain the same. As such, we can recycle cutting planes across subsequent block updates.

Consider two subsequent block updates of tree $t \in \mathcal{T}$. Let $\mathbf{z^t}$ be a feasible solution for Problem (6) obtained while applying Algorithm 3 during the first block update. This feasible solution corresponds to cutting plane $\nu \geq q_{\mathbf{r}}(\mathbf{z^t}) + \nabla q_{\mathbf{r}}(\mathbf{z^t})(\mathbf{z} - \mathbf{z^t})$. Solution $\mathbf{z^t}$ is also feasible for Problem (6) during the subsequent second update, with residual vector $\mathbf{r'}$.

Importantly, we can obtain $q_{\mathbf{r'}}(\mathbf{z^t})$ and $\nabla q_{\mathbf{r'}}(\mathbf{z^t})$ efficiently by caching the LU decomposition of the regularized Hessian matrix required to compute $q_{\mathbf{r}}(\mathbf{z^t})$ and $\nabla q_{\mathbf{r'}}(\mathbf{z^t})$ during the first update. As a result, we obtain cutting plane: $\nu^{(h)} \geq q_{\mathbf{r'}}(\mathbf{z^t}) + \nabla q_{\mathbf{r'}}(\mathbf{z^t})(\mathbf{z} - \mathbf{z^t})$ for little computational cost during the second update. We discuss the full technical details of this procedure in §C.1.3 of the appendix. Our cutting plane recycling procedure significantly reduces the number of OA iterations, solves of ILP (7), required to solve Problem (6) to optimality each time a block is updated in Algorithm (2). We show an example in panel A of Figure 8; the histogram shows the distribution of the number of ILP solves needed in Algorithm (2), comparing runs with and without our cutting plane recycling procedure.

Active Set Optimization: We also use this active set procedure to reduce the number of CBCD update performed in Algorithm 2. We first conduct block updates across a few sweeps of trees $t \in \mathcal{T}$ in order to identify an active set \mathcal{A} of blocks such that $\mathbf{z}^{\mathbf{t}} \neq \mathbf{0}$, $\forall t \in \mathcal{A}$. On this active set, we cyclically update blocks $t \in \mathcal{A}$ until the objective no longer improves. We then update all blocks $t \in \mathcal{T}$ to update our active set, terminating our algorithm when the active set no longer changes. We show a visualization of the effect of this procedure in panel B of Figure 8. The plot shows the objective function of Problem (4) during our CBCD algorithm, comparing runs with and without our active set procedure.

Efficient Regularization Paths: Finally, we present a procedure to efficiently compute regularization paths, i.e., sequences of solutions for Problem (4) with varying sparsities, computed across a range of λ values. Given a descending sequence of λ values, we apply Algorithm 2 repeatedly. We use the solution obtained by each application of Algorithm 2 to warm start the subsequent solve. We also apply the cutting plane recycling method discussed in the section above each time we update tree $t \in \mathcal{T}$. These procedures reduce the number of CBCD updates and ILP updates required to compute regularization paths. We show a visualization of the effect of this procedure in panel C in Figure 8; the histograms show the distribution of the number of ILP solves required to compute each solution along

the regularization path, comparing runs with and without our method.

3.2.2 Discussion

With our computational enhancements (§3.2.1), our CBCD algorithm scales to large problem sizes. For example, consider a boosting ensemble of 500 depth 7 trees, fit on the WIND dataset from Haslett and Raftery (1989), which has 6500 observations—the resulting ensemble has over 95000 nodes. Our CBCD algorithm can find high-quality solutions in less than **30 seconds**, and, moreover, can compute the regularization path of solutions of varying sparsities in less than 4 minutes. In §5.2, we present an experiment that evaluates the computation time of our approximate algorithm for computing regularization paths.

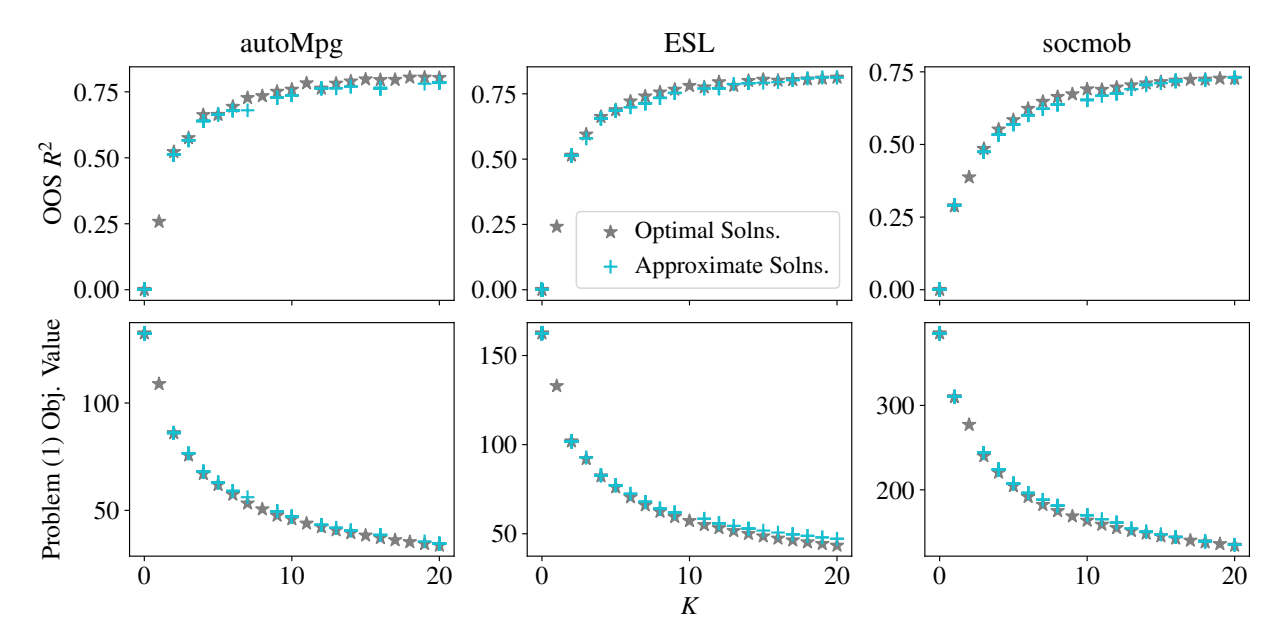


Figure 9: Comparison of solutions obtained by our optimal and approximate algorithms. The top plots show out-of-sample \mathbb{R}^2 vs. K and the bottom plots show the objective value of Problem (1) for each solution.

Importantly, we observe that our approximate algorithm obtains high-quality solutions along the regularization path which, although worse than those obtained by our exact algorithm, remain practically useful in real-world settings. In Figure 9, we apply our exact Algorithm 1 and approximate Algorithm 2 to prune tree ensembles consisting of 100 depth 3 decision trees, fit on the AUTOMPG, ESL, and SOCMOB datasets obtained from the

OpenML repository (Bischl et al., 2017). For both algorithms, we compute solutions along the regularization path for $K \in \{1, 2, ..., 20\}$. The top row of plots in Figure 9 shows the out-of-sample R^2 scores of the solutions as a function of K; optimal solutions are marked by grey stars, and approximate solutions are indicated by teal crosses. The bottom row of plots shows the corresponding objective value of Problem (1) for each solution. We observe that the solutions produced by our approximate algorithm are slightly worse in terms of both out-of-sample accuracy and the objective value of Problem (1). Nevertheless, the approximate solutions are sufficiently close to optimal solutions to remain useful in practice. Finally, because CBCD Algorithm 2 can become stuck in local minima, our approximate algorithm may occasionally fail to yield a solution for every model size K along the regularization path, a limitation that our exact algorithm avoids.

4 Statistical Theory

In this section, we derive non-asymptotic prediction error bounds for our estimator, illustrating that in large samples, our approach performs similarly to the oracle that chooses the best linear combination of the rules in the ensemble. The proofs of all the results in this section are provided in Appendix E.

Introduction. We assume the model $y_i = f^*(\mathbf{x}_i) + \epsilon_i$ for our training data $\{(y_i, \mathbf{x}_i)\}_{i=1}^n$, where n is the sample size, p is the number of features/predictors, $f^* : \mathbb{R}^p \to \mathbb{R}$ is the true regression function, \mathbf{x}_i is the feature vector for the i-th observation, and ϵ_i are independent $N(0, \sigma^2)$ with $\sigma > 0$. For concreteness, we focus on the case of deterministic design.

For our theoretical analysis, we assume that we have a binary tree ensemble constructed using the training data. We apply our proposed approach on the *same* training data and prune the ensemble by solving Problem (1). We do not make assumptions about the specific method that was used to construct the tree ensemble. For example, the ensemble could come from a gradient boosting or a random forest procedure.

Recall that the prediction vector of a solution to Problem (1) is given by a linear combination $\sum_{t\in\mathcal{T}}\sum_{j\in\mathcal{N}_t}\mathbf{M}_j^tw_j^t$. The elements of \mathbf{M}_j^t corresponding to the observations in node j of tree t are equal to the average response at the node, and the remaining elements are zero. Coefficients w_j^t uniquely determine the corresponding regression function $f: \mathbb{R}^p \to \mathbb{R}$, obtained by replacing each \mathbf{M}_j^t with the underlying rescaled indicator function², or rules, which we denote by r_j^t . Thus, each candidate regression function is given by $f(\mathbf{x}) = \sum_{t\in\mathcal{T}} \sum_{j\in\mathcal{N}_t} r_j^t(\mathbf{x}) w_j^t$.

Notation. Problem (1) imposes constraints on f, specifying the class of candidate regression functions. Depending on the choice of the attributes a_j^t used in the constraints, we denote the corresponding functional classes as $C_1(K)$, $C_2(K)$, or $C_3(K)$. We focus on the three attribute choices described in Section 2.2.2, i.e., (1) $a_j^t \equiv 1$; (2) $a_j^t =$ depth of node j in tree t; and (3) $a_j^t =$ number of distinct features used in rule r_j^t .

We observe the following relationship between the functional classes: $C_1(K) \supseteq C_3(K) \supseteq C_2(K)$. We write \hat{f}_1 , \hat{f}_2 and \hat{f}_3 for the estimated regression functions corresponding to each of the three classes and assume that these estimates are obtained by solving Problem (1) to global optimality.

We write \lesssim and \gtrsim to indicate that inequalities \lesssim and \gtrsim , respectively, hold up to positive universal multiplicative factors. We let D denote the maximum depth of the trees in the ensemble. In practice, D is often specified during the construction of the ensemble and used as the depth of every tree. We note that we allow both p and D to depend on n.

Given a candidate regression function $f(\mathbf{x}) = \sum_{t \in \mathcal{T}} \sum_{j \in \mathcal{N}_t} r_j^t(\mathbf{x}) w_j^t$, we write ||w(f)|| for the Euclidean norm of the coefficient vector, i.e., $||w(f)||^2 = \sum_{t \in \mathcal{T}} \sum_{j \in \mathcal{N}_t} (w_j^t)^2$. Similarly, we define $||w(f)||_{\infty} = \max_{t \in \mathcal{T}, j \in \mathcal{N}_t} |w_j^t|$. We also write $||f||_n$ for the empirical L_2 norm of f, i.e., $||f||_n^2 = \sum_{i=1}^n f^2(\mathbf{x}_i)/n$.

Results. The following theorem establishes non-asymptotic bounds on the prediction error,

²The indicator is used to specify the node, and the multiplier equals the average observed response for the node.

 $\|\widehat{f}_k - f^*\|_n^2$, for k = 1, 2, 3, comparing the predictive performance of our approach with that of an oracle, which chooses the best possible (data-dependent) coefficients w_j^t in the linear combination $\sum_{t \in \mathcal{T}} \sum_{j \in \mathcal{N}_t} r_j^t(\mathbf{x}) w_j^t$ under the imposed constraint on the attributes. We treat the attribute budget K as a user-supplied value rather than a parameter that we tune.

Theorem 1. Let $\delta_0 \in (0,1)$. Then,

$$\|\widehat{f}_1 - f^*\|_n^2 \lesssim \inf_{f_1 \in \mathcal{C}_1(K)} \left\{ \|f_1 - f^*\|_n^2 + \frac{1}{n\gamma} \|w(f_1)\|^2 \right\} + \sigma^2 \frac{KD \log(enp) - \log(\delta_0)}{n}$$

$$\|\widehat{f}_2 - f^*\|_n^2 \lesssim \inf_{f_2 \in \mathcal{C}_2(K)} \left\{ \|f_2 - f^*\|_n^2 + \frac{1}{n\gamma} \|w(f_2)\|^2 \right\} + \sigma^2 \frac{K \log(enp) - \log(\delta_0)}{n}$$

$$\|\widehat{f}_3 - f^*\|_n^2 \lesssim \inf_{f_3 \in \mathcal{C}_3(K)} \left\{ \|f_3 - f^*\|_n^2 + \frac{1}{n\gamma} \|w(f_3)\|^2 \right\} + \sigma^2 \frac{K \log(enp) - \log(\delta_0)}{n},$$

with probability at least $1 - \delta_0$.

Remark 1. It is interesting to note that there is no obvious "true" linear combination of the rules $r_j^t(\mathbf{x})$, which would serve as a natural target for our estimators. This phenomenon occurs because the rules are constructed using the training data via ensemble methods such as gradient boosting or random forests. We overcome this issue by comparing our estimators with the **best** possible linear combination of the rules $r_i^t(\mathbf{x})$.

Remark 2. We note that the functions in classes $C_k(K)$ are random, because the rules $r_i^t(\mathbf{x})$ are constructed from the training data. Thus, the inf on the right-hand sides of the bounds in Theorem 1 is computed pointwise, i.e., for every training sample. In other words, the oracle coefficients in the linear combination of the rules depend on the tree ensemble.

Remark 3. We emphasize that we do not impose any assumptions on the method that was used to construct our tree ensemble.

Remark 4. We are not aware of other existing prediction error bounds for ensemble pruning algorithms.

The following result illustrates the prediction error rates in the case where a good approximation to f^* can be achieved via an oracle linear combination of the rules.

Corollary 1. Let $r_1 = KD \log(enp)/n$ and $r_2 = r_3 = K \log(enp)/n$. Suppose that, for some universal constant c, inequality

$$\inf_{\substack{f \in \mathcal{C}_k(K) \\ \|w(f)\|_{\infty} \le c}} \|f - f^*\|_n^2 \lesssim \sigma^2 r_k$$

holds with probability at least $1 - \epsilon$ for some $\epsilon \in (0, 1)$ and $k \in \{1, 2, 3\}$. Let $\delta_1 = (enp)^{-KD}$ and $\delta_2 = \delta_3 = (enp)^{-K}$. Then, with probability at least $1 - \delta_k - \epsilon$, inequality

$$\|\widehat{f}_k - f^*\|_p^2 \lesssim \sigma^2 r_k$$

holds provided that $\gamma \gtrsim K(\sigma^2 n r_k)^{-1}$.

Remark 5. Probability $1 - \delta_k$ is high as long as either n or p is large. In particular, $n \lor p \to \infty$ implies $\delta_k \to 0$ for each $k \in \{1, 2, 3\}$.

Remark 6. Probability $1 - \epsilon$ is high if a good approximation to f^* is likely to be achieved via an oracle linear combination of the rules in the ensemble within the imposed attribute budget. Such an approximation would be a consequence of (i) existence of a good corresponding approximation to f^* using deterministic rules; and (ii) high overall quality of the collection of rules provided by the tree ensemble.

Remark 7. The assumption $||w(f)||_{\infty} \leq c$ imposed on the oracle appears to be mild. Recall that the prediction of each rule $r_j^t(\mathbf{x})$ equals the average observed response for the corresponding node. Thus, it is reasonable to believe that good linear combinations of the rules would have uniformly bounded non-negative coefficients.

Remark 8. Recall that we add the ridge penalty to the Problem (1) objective for computational reasons, and we set the penalty weight $1/\gamma$ to a small positive value. This approach

is consistent with the conditions of Corollary 1, which require that γ is sufficiently large.

Remark 9. We note that $r_1 \geq r_2 = r_3$ and $r_1/r_2 = D$. Consequently, both the depthweighting scheme and the feature-weighting scheme may significantly improve over the rule-weighting scheme when the trees in the ensemble are deep and the true regression function can be well approximated using the allocated attribute budget. This observation is consistent with the results in Figure 7.

The error rates in Corollary 1 can also apply to approximate solutions obtained after an early termination of the MIP solver. Upon termination, the solver provides the upper and lower bounds on the value of the objective function. We denote these bounds by UB and LB, respectively, and write $\tau = (UB - LB)/UB$ for the corresponding optimality gap. Let \tilde{f}_k , with $k \in \{1,2,3\}$, denote the approximate solutions produced by the solver for Problem (1) with our three attribute choices, respectively. The following result demonstrates that the bounds in Corollary 1 hold for the approximate solution \tilde{f}_k when τ is bounded away from one and $\tau \lesssim r_k$.

Corollary 2. Suppose that $\tau \leq 1 - a$ for some positive universal constant a. Then, under the assumptions of Corollary 1, inequality

$$\|\widetilde{f}_k - f^*\|_n^2 \lesssim \sigma^2 r_k + \sigma^2 \tau$$

holds with probability at least $1 - \delta_k - \epsilon$, provided that $\gamma \gtrsim K(\sigma^2 n r_k)^{-1}$.

5 Experiments

In this section, we evaluate our proposed estimator in terms of computational efficiency and predictive performance.

5.1 Computation Time: Exact Algorithm

We first evaluate the computation time of our proposed exact algorithm (Algorithm 1) against two state-of-the art commercial solvers, Gurobi and MOSEK, by solving various size instances of Problem (1). For each instance, we extract a set of K = 20 decision rules, a typical use case for our framework. The results of this timing experiment are presented in Table 1. We show the computation time of each method averaged over 5 runs, with standard errors shown in parentheses. The left two columns of the table report ensemble size, specified by the number of trees and depth, and the size of Problem (1), specified by the number of observations and binary decision variables. Cells highlighted in red indicate instances where the method fails to find the optimal solution within the 3-hour time limit.

Ensemble Size	Problem Size	Proposed Exact	Gurobi	MOSEK
# Trees / Depth	Obs. / Binary Vars.	Algorithm		
100 / 3	1000 / 1500	1.69s (0.04)	>3h	>3h
100 / 5	1000 / 5000	7.64s (0.14)	>3h	>3h
500 / 4	1000 / 10000	14.2s (0.18)	>3h	>3h
100 / 3	3000 / 1500	8.8s (0.15)	>3h	>3h
100 / 5	3000 / 5000	18.3s (0.18)	>3h	>3h
500 / 4	3000 / 10000	38.1s (0.42)	>3h	>3h
100 / 3	5000 / 1500	164.8s (1.23)	>3h	>3h
100 / 5	5000 / 5000	247.49s (2.45)	>3h	>3h
500 / 4	5000 / 10000	10m 21s (10.41)	>3h	>3h
100 / 3	10000 / 1500	6m 39s (12.50)	>3h	>3h
100 / 5	10000 / 5000	41m 21s (6.19)	>3h	>3h
500 / 4	10000 / 10000	58m 30s (10.65)	>3h	>3h

Table 1: Computation time for a single solve of Problem (1) using our exact algorithm.

From Table 1, we observe that our optimal algorithm significantly outperforms commercial solvers in solving Problem (1). Even for the smallest instance of Problem (1) considered, both Gurobi and MOSEK fail to find an optimal solution within a 3-hour time limit. In contrast, our tailored algorithm typically identifies the optimal solution within seconds to minutes. This timing experiment demonstrates that solving Problem (1) to optimality using our exact algorithm is practical for a wide range of problem sizes. In the next section, we assess the computational efficiency of our approximate algorithm when

5.2 Computation Time: Regularization Paths

Ensemble Size	Problem Size	Approximate	w/o Computational	
# Trees / Depth	Obs. / Binary Vars.	Algorithm	Enhancements	
500 / 4	5000 / 10000	45s (0.79)	>3h	
300 / 5	5000 / 15000	1m 7s (1.54)	>3h	
600 / 5	5000 / 30000	1m 32s (1.40)	>3h	
500 / 6	5000 / 50000	2m 51s (4.12)	>3h	
500 / 7	5000 / 100000	3m 30s (6.91)	>3h	
500 / 4	10000 / 10000	52.4s (0.77)	>3h	
300 / 5	10000 / 15000	1m 17s (1.37)	>3h	
600 / 5	10000 / 30000	2m 5s (4.53)	>3h	
500 / 6	10000 / 50000	2m 57s (6.12)	>3h	
500 / 7	10000 / 100000	3m 59s (7.41)	>3h	
500 / 4	15000 / 10000	1m 33s (2.33)	>3h	
300 / 5	15000 / 15000	1m 57s (3.12)	>3h	
600 / 5	15000 / 30000	2m 51s (3.51)	>3h	
500 / 6	15000 / 50000	3m 56s (8.49)	>3h	
500 / 7	15000 / 100000	4m 59s (10.48)	>3h	

Table 2: Computation time required to generate the regularization path for 50 values of λ . The rightmost column reports runtimes without the enhancements described in §3.2.1.

We use this procedure to evaluate the computational efficiency of our approximate algorithm for computing regularization paths. For various size instances of Problem (4), we apply Algorithm 2 across 50 values of λ , evenly spaced on a logarithmic scale from 10^0 to 10^3 . We incorporate the computational enhancements discussed in §3.2.1 and record the total time required to compute the full regularization path. This yields a sequence of solutions to Problem (1) with varying sparsity levels, corresponding to rule sets of different sizes. For comparison, we also run Algorithm 2 without the enhancements from §3.2.1, using Gurobi to solve Problem (5) at each block update.

The results of this timing experiment are reported in Table 2, where we show the computation time of each method averaged across 5 runs (the standard errors are shown in parentheses). The left two columns report the ensemble size and the dimensions of each instance of Problem (4), specified by the number of observations and binary decision

variables (i.e., nodes in the tree ensemble). The smallest instance considered, 5,000 observations and 10,000 binary decision variables, matches the largest problem size evaluated in our timing experiments for the exact algorithm (§5.1). In this experiment, we scale to significantly larger ensembles, evaluating regularization paths for problems with up to 100,000 binary decision variables. Table 2 shows that our approximate algorithm (Algorithm 2), when combined with the computational enhancements from §3.2.1, is able to compute regularization paths across all problem sizes within minutes. In contrast, without these enhancements, the algorithm fails to compute any regularization path within three hours. These results demonstrate that our enhanced approximate algorithm can efficiently compute regularization paths for large-scale instances of Problem (4).

5.3 Predictive Performance

In this section, we evaluate how well our estimator performs at extracting interpretable sets of decision rules from tree ensembles. We follow the experimental procedure discussed below on 25 regression datasets from the OpenML repository (Bischl et al., 2017), and the full list of datasets along with metadata can be found in §F.1 of the appendix.

Experimental Procedure For each dataset, we perform 5-fold cross-validation. On the training folds, we fit gradient boosting tree ensembles with maximum depths of $\{3, 5, 7\}$ and for each ensemble, we apply our estimator and use Algorithm 2 to compute regularization paths. Along each path, we extract sets of $K = \{10, 15, 20, 25\}$ decision rules and evaluate the out-of-sample R^2 of the resulting compact models. We restrict our extracted rule sets to have no more than 25 rules to preserve interpretability, so that the rules can be examined by hand. We compare the performance of our framework against these competing algorithms. RuleFit (Friedman and Popescu, 2008), which uses the LASSO to select decision rules without pruning depth. FIRE (Liu and Mazumder, 2023a), which uses a sparsity-inducing MCP-penalty to select rules without pruning rule depth. ForestPrune

(Liu and Mazumder, 2023b), which selects trees and prunes depths without explicitly selecting rules. **ISLE** (Friedman et al., 2003), which uses the LASSO to select trees. For each competing method, we compute regularization paths and extract models with at most $K = \{10, 15, 20, 25\}$ decision rules, or leaf nodes for ISLE and ForestPrune. We compare the out-of-sample \mathbb{R}^2 of these models against the compact models obtained by our framework, and we show a visualization of this experiment in Figure 10.

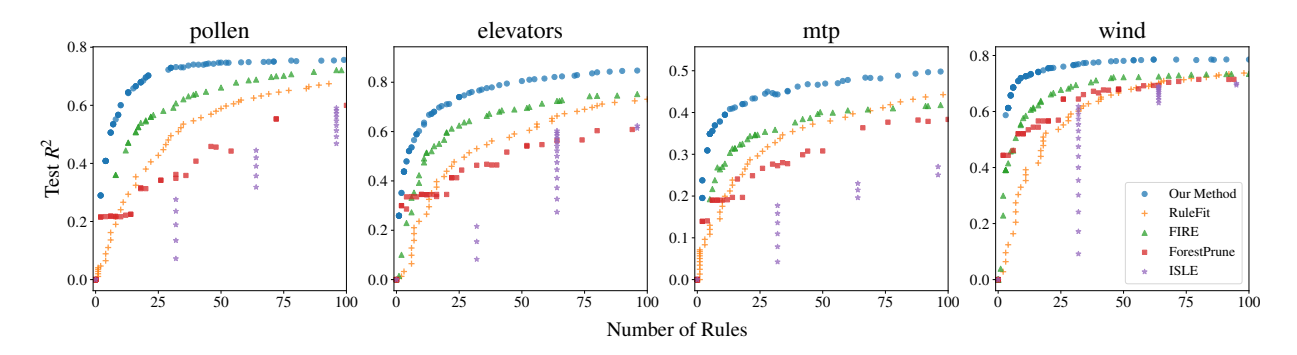


Figure 10: Visualization of regularization paths for all methods in our experiment on 4 datasets from OpenML (Bischl et al., 2017). The horizontal axes show the number of rules extracted and the vertical axis shows out-of-sample \mathbb{R}^2 .

Experimental Results: Across all datasets, folds, ensemble depths, and budgets of rules K, we compare the out-of-sample R^2 of our framework against our competing methods. We report the percent increase in out-of-sample R^2 between our framework and our competing algorithms, defined by: (Our Method R^2 -Competing Method R^2)/(Competing Method R^2). Percent increases above 0 indicate that our method outperforms the competing algorithm.

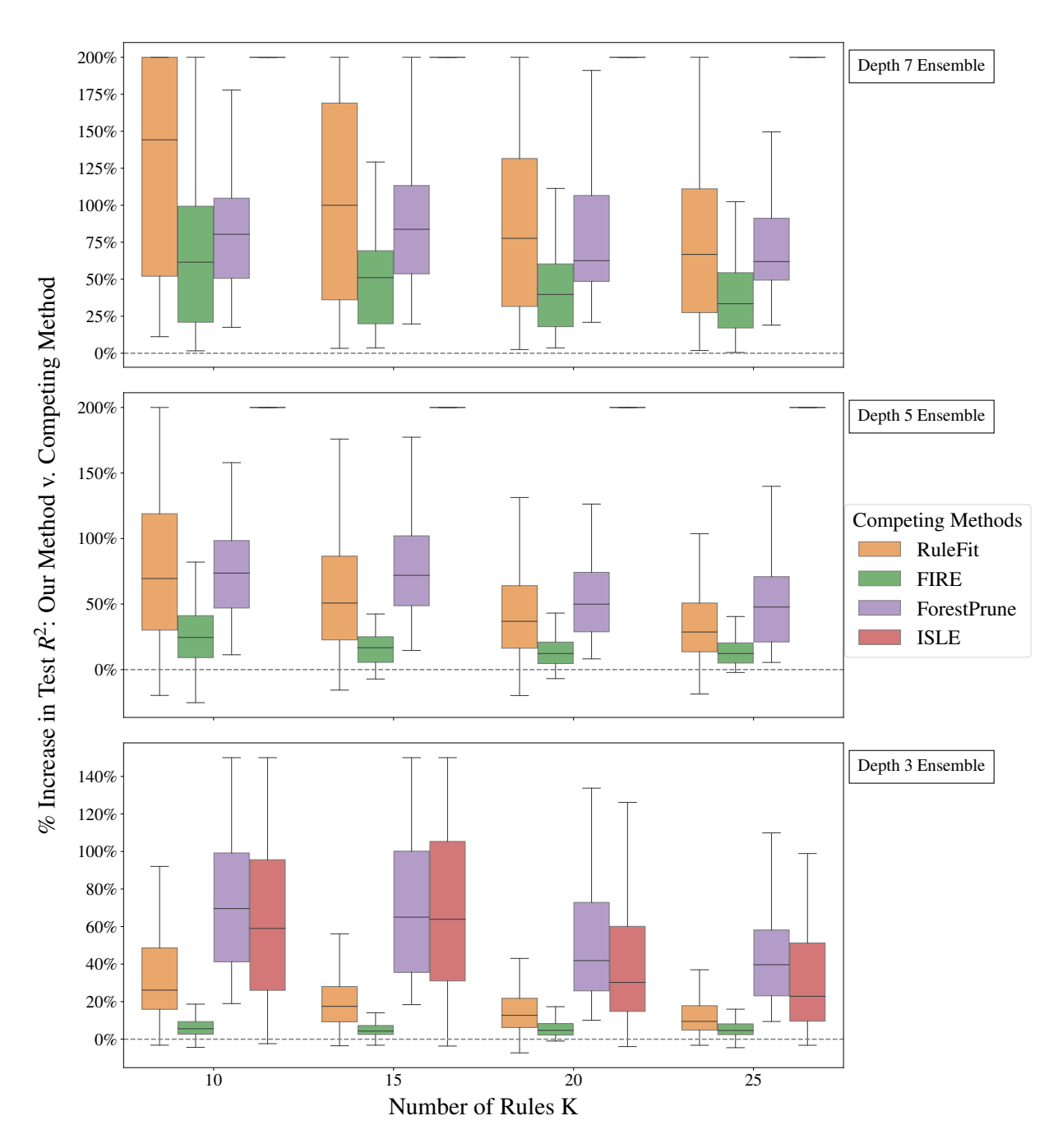


Figure 11: Experimental results for extracting interpretable rule sets. The horizontal axis shows the budget on the number of rules and the vertical axes show the percent increase in test R^2 between our algorithm and the competing methods. Percent increases above 0 (indicated by the dashed line) show that our algorithm outperforms the competing method.

In Figure 11, we show the distribution of these results across all datasets and folds in our experiment. Each panel in the figure shows results for a different ensemble depth, $\{3,5,7\}$. The horizontal axes in each panel shows K, the budget on the number of rules, and the vertical axes show the percent increase between our algorithm and our competing methods. The box-plots are color-coded by competing method and show the distribution of percent increases across all datasets and folds.

We observe that our estimator consistently outperforms competing methods in constructing interpretable rule sets; the interquartile ranges of all box plots in Figure 11 are strictly positive. Compared to the best-performing competing method, FIRE, our approach achieves approximately a 50%, 20%, and 8% increase in out-of-sample R^2 when extracting rule sets from ensembles of depths 7, 5, and 3, respectively. Our method also shows increasing performance gains over RuleFit and FIRE as ensemble depth increases, owing to its ability to prune rule depth. In contrast, these competing methods are limited to extracting sets of high-depth rules, which tend to perform poorly. In addition, ForestPrune performs poorly due to its limited flexibility: it can only prune tree depth and cannot extract decision rules from trees, which restricts its effectiveness in producing sparse rule sets. Finally we note that ISLE fails to extract sparse rule sets when ensemble depth is greater than 3. A single tree of depth 5 already contains more than 25 rules, so we omit ISLE from the depth 5 and depth 7 displays. These results demonstrate that our method significantly outperforms competing algorithms in extracting sparse, interpretable rule sets.

5.3.1 Model Compression

Finally, we evaluate how well our algorithm performs at compressing large tree ensembles, which is useful for reducing inference time and memory footprint.

Experimental Procedure: On each of the 25 OpenML datasets from above, we conduct a 5-fold cross validation and further split each training fold into a training set and a

validation set. On the training sets, we fit large boosting ensembles consisting of 500 depth 7 decision trees; such ensembles typically contain around 10^5 nodes. We then apply our framework to prune these ensembles by computing regularization paths and selecting the smallest pruned model that achieves a validation R^2 within a prespecified margin $\phi \in \{1\%, 2.5\%, 5\%, \dots, 20\%\}$ of the full model. Here, ϕ serves as a tuning parameter in the compression procedure. We evaluate the test R^2 and size of the selected pruned model.

We report the following metrics: the percentage decrease in test R^2 between our pruned model and the full model, given by: (Full Model R^2 – Pruned Model R^2)/(Full Model R^2), and the compression factor, given by: (# Nodes Full Model)/(# Nodes Pruned Model). Finally, we repeat this procedure using FIRE, RuleFit, ForestPrune, and ISLE.

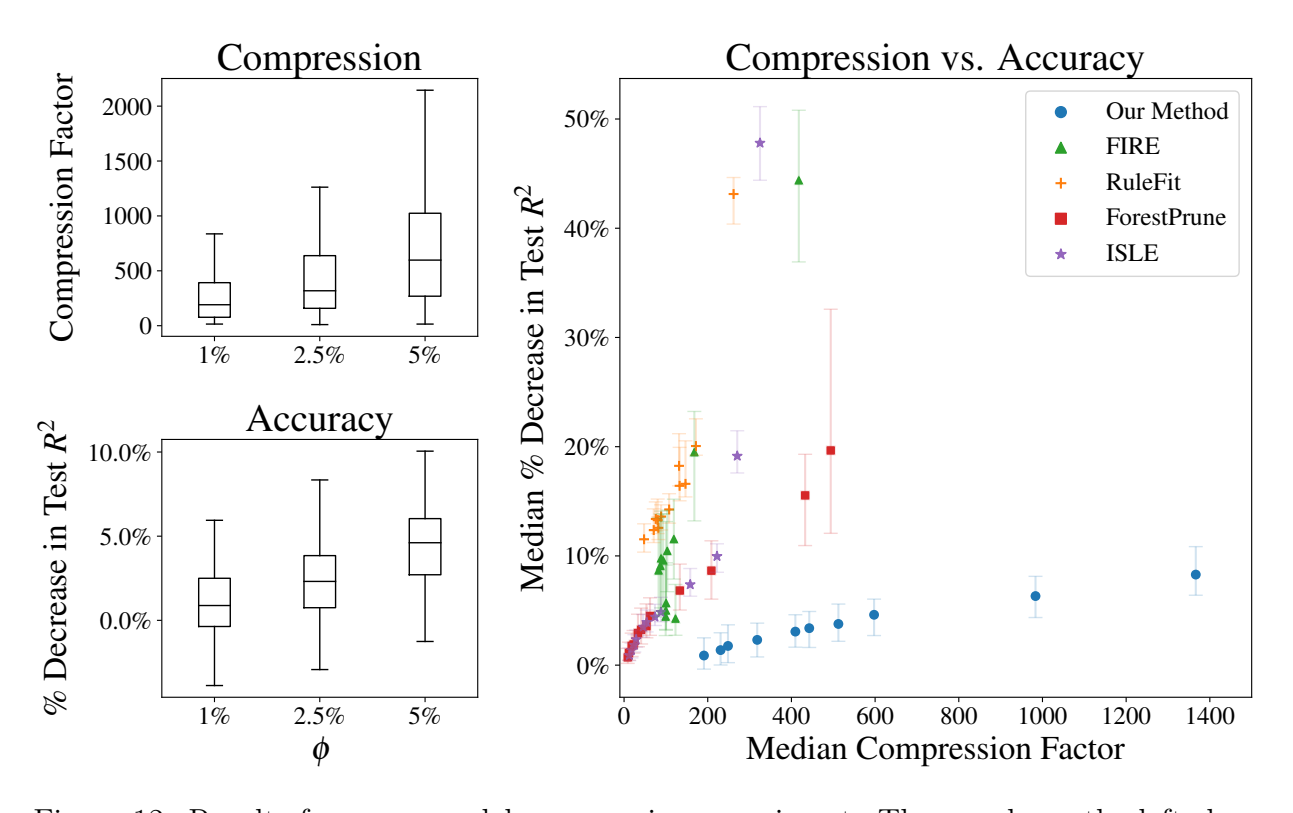


Figure 12: Results from our model compression experiment. The panels on the left show the distributions of the compression factor and the percentage decrease in test R^2 between our pruned model and the full model, obtained across all datasets and folds. The right panel compares the performance of our pruning method against competing algorithms.

Experimental Results: We show the results of our experiment in Figure 12. In the left and center panels, we display boxplots of the distributions of the compression factor (top

left) and the percentage decrease in test R^2 (bottom left) between our pruned model and the full model, across all datasets and folds, for $\phi \in \{1\%, 2.5\%, 5\%\}$. For the $\phi = 1\%$ setting, our method achieves a median compression factor of $190\times$ relative to the full model, while incurring only a median decrease in test R^2 of 0.8%. For the $\phi = 2.5\%$ and $\phi = 5\%$ settings, our method can prune models on median $300\times$ and $600\times$ times smaller than the full model, while incurring a median decrease in test R^2 of 2.3% and 4.6%, respectively. These results show that our method can compress large ensembles by factors exceeding two orders of magnitude, while incurring only nominal losses in predictive accuracy.

The right panel in Figure 12 compares our method against the competing algorithms, across all values of ϕ in our experiment. The horizontal axis shows the median compression factor obtained by each method (higher is better), and the vertical axis shows the median percentage decrease in test R^2 between the pruned models and the full model (lower is better). We observe that our method achieves significantly higher compression factors with lower decreases in test R^2 compared to all competing algorithms. Notably, we can prune models to nearly $1400 \times$ smaller than the original boosting ensemble while retaining out-of-sample R^2 scores within 10% of the full model. These results demonstrate that our method achieves significantly better compression of large models than competing algorithms.

References

Belgiu, M., and Drăguţ, L. (2016), "Random forest in remote sensing: A review of applications and future directions," *ISPRS journal of photogrammetry and remote sensing*.

Bertsimas, D., and Van Parys, B. (2020), "Sparse high-dimensional regression," *The Annals of Statistics*, 48, 300–323.

Biblarz, T. J., and Raftery, A. E. (1993), "The effects of family disruption on social mobility," *American sociological review*, 97–109.

Bischl, B., Casalicchio, G., Feurer, M., Gijsbers, P., Hutter, F., Lang, M., Mantovani, R. G., van Rijn, J. N., and Vanschoren, J. (2017), "Openml benchmarking suites," arXiv preprint arXiv:1708.03731.

Boyd, S. P., and Vandenberghe, L. (2004), *Convex optimization*, Cambridge university press.

Breiman, L. (2001a), "Random forests," Machine learning, 45, 5–32.

- (2001b), "Statistical modeling: The two cultures (with comments and a rejoinder by the author)," *Statistical science*, 16, 199–231.
- Bühlmann, P., and Van De Geer, S. (2011), Statistics for high-dimensional data: methods, theory and applications, Springer Science & Business Media.
- Chen, X., and Ishwaran, H. (2012), "Random forests for genomic data analysis," Genomics.
- Davern, M., Bautista, R., Freese, J., Herd, P., and Morgan, S. L. (2024), "General Social Survey 1972-2024," NORC ed. Chicago.
- Duran, M. A., and Grossmann, I. E. (1986), "An outer-approximation algorithm for a class of mixed-integer nonlinear programs," *Mathematical programming*, 36, 307–339.
- Efron, B., and Hastie, T. (2021), Computer age statistical inference, student edition: algorithms, evidence, and data science, vol. 6, Cambridge University Press.
- Fletcher, R., and Leyffer, S. (1994), "Solving mixed integer nonlinear programs by outer approximation," *Mathematical programming*, 66, 327–349.
- Friedman, J. H. (2002), "Stochastic gradient boosting," Computational statistics & data analysis, 38, 367–378.
- Friedman, J. H., and Popescu, B. E. (2008), "Predictive learning via rule ensembles," .
- Friedman, J. H., Popescu, B. E. et al. (2003), "Importance sampled learning ensembles," *Journal of Machine Learning Research*, 94305, 1–32.
- Gurobi Optimization, LLC (2024), Gurobi Optimizer Reference Manual.
- Haslett, J., and Raftery, A. E. (1989), "Space-time modelling with long-memory dependence: Assessing Ireland's wind power resource," *Journal of the Royal Statistical Society:* Series C (Applied Statistics), 38, 1–21.
- Hazimeh, H., Mazumder, R., and Radchenko, P. (2023), "Grouped variable selection with discrete optimization: Computational and statistical perspectives," *The Annals of Statistics*, 51, 1–32.
- Liu, B., and Mazumder, R. (2023a), "Fire: An optimization approach for fast interpretable rule extraction," in *Proceedings of the 29th ACM SIGKDD Conference on Knowledge Discovery and Data Mining*, pp. 1396–1405.
- Liu, B.— (2023b), "Forestprune: Compact depth-pruned tree ensembles," in *International Conference on Artificial Intelligence and Statistics*, PMLR, pp. 9417–9428.
- Mazumder, R., Radchenko, P., and Dedieu, A. (2023), "Subset selection with shrinkage: Sparse linear modeling when the SNR is low," *Operations Research*, 71, 129–147.
- Meinshausen, N. (2010), "Node harvest," The Annals of Applied Statistics, 2049–2072.
- MOSEK ApS (2024), MOSEK Optimizer API Manual.
- Petersen, K. B., Pedersen, M. S. et al. (2008), "The matrix cookbook," *Technical University of Denmark*, 7, 510.
- Pferschy, U., and Schauer, J. (2009), "The knapsack problem with conflict graphs," *Journal of Graph Algorithms and Applications*, 13, 233–249.
- Shwartz-Ziv, R., and Armon, A. (2022), "Tabular data: Deep learning is not all you need," *Information Fusion*, 81, 84–90.

A Related Work Discussion

We discuss additional details on existing ensemble pruning algorithms and highlight the advantages of our proposed estimator.

As mentioned in §1.1, the paper Importance Sampled Learning Ensembles (Friedman et al., 2003), ISLE, introduces one of the earliest computational approaches to prune tree ensembles. Consider an ensemble of T decision trees, $\{\Gamma_1, \dots \Gamma_T\}$ and let Γ_t denote the vector of predictions for the tree Γ_t . ISLE uses this optimization problem to prune trees: $\min_{\boldsymbol{\beta}} ||\mathbf{y} - \sum_{t=1}^T \beta_t \Gamma_t||_2^2 + \lambda ||\boldsymbol{\beta}||_1$, where $\mathbf{y} \in \mathbb{R}^n$ is the response vector and λ is the weight for the LASSO penalty that encourages sparsity in trees. The method is only able to extract entire trees from the ensemble, and cannot prune interaction depth or individual rules.

RuleFit (Friedman and Popescu, 2008) deconstructs a tree ensemble into a large collection of m' decision rules and uses the LASSO to extract a sparse subset of rules: $\min_{\boldsymbol{\beta}} ||\mathbf{y} - \sum_{j=1}^{m'} \beta_j \mathbf{r}_j||_2^2 + \lambda ||\boldsymbol{\beta}||_1$, where $\mathbf{r}_j \in \mathbb{R}^n$ is the prediction vector for the rule r_j . A similar procedure, Node Harvest (Meinshausen, 2010) uses the non-negative garrote to sparsify rules. Both of these algorithms struggle to scale to larger problem sizes, e.g., ensembles of depth greater than 4, as shown in the empirical results of Liu and Mazumder (2023a). Moreover, neither method prunes interaction depth; the extracted rules retain the same depth as those in the original tree ensemble.

FIRE (Liu and Mazumder, 2023a) uses this optimization framework to extract rules $\min_{\beta} |\mathbf{y} - \sum_{j=1}^{m'} \beta_j \mathbf{r}_j|_2^2 + h(\beta, \lambda)$, where $h(\beta, \lambda)$ is a non-convex, sparsity-inducing penalty, such as the minimax concave penalty, and greedy optimization techniques are used to improve computation. FIRE scales to pruning larger and deeper ensembles than RuleFit and Node Harvest, and achieves better predictive performance, as demonstrated in Liu and Mazumder (2023a). However, FIRE does not prune rule depth, and its optimization formulation cannot be readily extended to do so.

Compared to these existing rule-pruning methods, our proposed estimator can support

interaction depth pruning, which greatly improves predictive performance as our experiments in §5.3 show. In addition, we provide theoretical guarantees for our estimator, which are not offered by existing methods.

ForestPrune (Liu and Mazumder, 2023b) is an algorithm designed to prune depth layers from tree ensembles. However, it is limited to pruning entire trees and cannot extract individual decision rules. Furthermore, its optimization framework—based on block coordinate descent over full trees—is not easily adaptable for rule extraction. While ForestPrune returns a collection of trees of varying depths, our goal is to extract a compact set of rules. The models produced by ForestPrune are typically larger and less flexible than those produced by our estimator, which supports both depth pruning and rule extraction. Consequently, our method significantly outperforms ForestPrune in extracting compact models in terms of predictive performance, as shown by our experiments in §5.3.Finally, ForestPrune lacks theoretical guarantees, in contrast to our estimator.

B Optimal Algorithm

B.1 Proof of Propositions

In this section, we present the proofs for the propositions used in our optimal algorithm.

B.1.1 Proof of Proposition 1

We prove here that Problem (2) is an equivalent reformulation of Problem (1). We display both of these problems below.

Problem (1):

$$\min_{z_i^t, w_i^t} \quad \frac{1}{2} \left\| \mathbf{y} - \sum_{t \in \mathcal{T}} \sum_{i \in \mathcal{N}_t} \mathbf{M}_i^t w_i^t \right\|_2^2 + \frac{1}{2\gamma} \sum_{t \in \mathcal{T}} \sum_{i \in \mathcal{N}_t} (w_i^t)^2$$
s.t.
$$\sum_{j \in \mathcal{C}_i^t} z_j^t \leq \left| \mathcal{C}_i^t \middle| z_i^t, \quad \forall \ i \in \mathcal{N}_t, \ t \in \mathcal{T},$$

$$\sum_{t \in \mathcal{T}} \sum_{i \in \mathcal{N}_t} a_i^t z_i^t \leq K,$$

$$(1 - z_i^t) \ w_i^t = 0, \quad \forall \ i \in \mathcal{N}_t, \ t \in \mathcal{T},$$

$$z_i^t \in \{0, 1\}, \quad \forall \ i \in \mathcal{N}_t, \ t \in \mathcal{T}.$$

Problem (2):

$$\min_{\mathbf{z}} \quad \frac{1}{2} \mathbf{y}^{\top} \left(\mathbb{I}_{n} + \gamma \sum_{t \in \mathcal{T}} \sum_{i \in \mathcal{N}_{t}} z_{i}^{t} \mathbf{M}_{i}^{t} (\mathbf{M}_{i}^{t})^{\top} \right)^{-1} \mathbf{y}$$
s.t.
$$\sum_{j \in \mathcal{C}_{i}^{t}} z_{j}^{t} \leq |\mathcal{C}_{i}^{t}| z_{i}^{t}, \quad \forall i \in \mathcal{N}_{t}, \ t \in \mathcal{T},$$

$$\sum_{t \in \mathcal{T}} \sum_{i \in \mathcal{N}_{t}} a_{i}^{t} z_{i}^{t} \leq K,$$

$$z_{i}^{t} \in \{0, 1\}, \quad \forall i \in \mathcal{N}_{t}, \ t \in \mathcal{T}.$$

Note that we use \mathbf{z} and w to refer to the decision vectors formed by stacking all z_i^t and w_i^t decision variables for all $i \in \mathcal{N}_t$ and $t \in \mathcal{T}$.

Consider some solution \mathbf{z}^* to Problem (2), with objective value:

$$\frac{1}{2}\mathbf{y}^{\top} \bigg(\mathbb{I}_n + \gamma \sum_{t \in \mathcal{T}} \sum_{i \in \mathcal{N}_t} (z_i^t)^* \mathbf{M}_i^t \big(\mathbf{M}_i^t\big)^{\top} \bigg)^{-1} \mathbf{y}$$

Note that solution \mathbf{z}^* satisfies the first, second, and fourth constraint in Problem (1). We fix decision variable \mathbf{z} to be \mathbf{z}^* in Problem (1) and minimize with respect to w. This is

given by:

$$\min_{\boldsymbol{w}_{i}^{t}} \quad \frac{1}{2} \left\| \mathbf{y} - \sum_{t \in \mathcal{T}} \sum_{i \in \mathcal{N}_{t}} \mathbf{M}_{i}^{t} \boldsymbol{w}_{i}^{t} \right\|_{2}^{2} + \frac{1}{2\gamma} \sum_{t \in \mathcal{T}} \sum_{i \in \mathcal{N}_{t}} (\boldsymbol{w}_{i}^{t})^{2}$$
s.t.
$$(1 - (\boldsymbol{z}_{i}^{t})^{*}) \boldsymbol{w}_{i}^{t} = 0, \quad \forall i \in \mathcal{N}_{t}, \ t \in \mathcal{T},$$

$$(\boldsymbol{z}_{i}^{t})^{*} \in \{0, 1\}, \quad \forall i \in \mathcal{N}_{t}, \ t \in \mathcal{T}.$$

Let \mathcal{M} denote the $n \times \left(\sum_{t \in \mathcal{T}} |\mathcal{N}_t|\right)$ matrix formed by taking the vectors \mathbf{M}_i^t as its columns. Let $S = \{i : z_i^* \neq 0\}$, and let \mathcal{M}_S be the sub-matrix of \mathcal{M} formed by selecting the columns corresponding to indices in S.

The non-zero coefficients, w_S^* , to the optimal solution of Problem (8), \mathbf{w}^* , are given by:

$$w_S^* = \left(\frac{\mathbb{I}_{|S|}}{\gamma} + \mathcal{M}_S^{\mathsf{T}} \mathcal{M}_S\right)^{-1} \mathcal{M}^{\mathsf{T}} \mathbf{y}.$$

In addition:

$$\mathcal{M}_S(\mathcal{M}_S)^{\top} = \sum_{t \in \mathcal{T}} \sum_{i \in \mathcal{N}_t} (z_i^t)^* \mathbf{M}_i^t (\mathbf{M}_i^t)^{\top}.$$
(9)

We plug in \mathbf{w}^* into the objective function for Problem (8) and apply the Woodbury matrix identity (Petersen et al., 2008). This yields:

$$\frac{1}{2} \left\| \mathbf{y} - \sum_{t \in \mathcal{T}} \sum_{i \in \mathcal{N}_t} \mathbf{M}_i^t (w_i^t)^* \right\|_2^2 + \frac{1}{2\gamma} \sum_{t \in \mathcal{T}} \sum_{i \in \mathcal{N}_t} \left((w_i^t)^* \right)^2 = \frac{1}{2} \mathbf{y}^\top \left(\mathbb{I}_n + \gamma \sum_{t \in \mathcal{T}} \sum_{i \in \mathcal{N}_t} (z_i^t)^* \mathbf{M}_i^t \left(\mathbf{M}_i^t \right)^\top \right)^{-1} \mathbf{y}$$

Any solution \mathbf{z}^* to Problem (2) corresponds to solution ($\mathbf{z}^*, \mathbf{w}^*$) to Problem (1), and the corresponding objective values are equal.

The reverse statement also holds. Consider some solution \mathbf{z}^* , \mathbf{w}^* to Problem (1); \mathbf{z}^* is a solution to Problem (2) and it is apparent that the objective values of these two solutions are identical. Therefore, Problem (2) is an equivalent reformulation of Problem (1).

B.1.2 Proof of Proposition 2

We prove that function $\mathbf{z} \mapsto q(\mathbf{z})$ where $q(\mathbf{z})$ is convex on $\mathbf{z} \in [0,1]^m$. We have that:

$$q(\mathbf{z}) = \frac{1}{2} \mathbf{y}^{\top} \left(\mathbb{I}_n + \gamma \sum_{t \in \mathcal{T}} \sum_{i \in \mathcal{N}_t} z_i^t \mathbf{M}_i^t (\mathbf{M}_i^t)^{\top} \right)^{-1} \mathbf{y}$$

We use this result; Example 3.4, Boyd and Vandenberghe (2004) states that function,

$$f(\boldsymbol{\alpha}, A) = \boldsymbol{\alpha}^{\top} A^{-1} \boldsymbol{\alpha}$$

is convex in $(\boldsymbol{\alpha}, A)$ where $\boldsymbol{\alpha} \in \mathbb{R}^n$ and A is a symmetric positive definite matrix of size $n \times n$. For our function $q(\mathbf{z})$, vector y is fixed. Matrix $\left(\mathbb{I}_n + \gamma \sum_{t \in \mathcal{T}} \sum_{i \in \mathcal{N}_t} z_i^t \mathbf{M}_i^t (\mathbf{M}_i^t)^\top\right)$ is positive definite and an affine function of \mathbf{z} . Function $q(\mathbf{z})$ is a convex composition of an affine function and is therefore convex over \mathbf{z} .

B.2 Objective and Subgradient Evaluation

We present here an efficient procedure to evaluate objective $q(\mathbf{z})$ and subgradient $\nabla q(\mathbf{z})$ for any solution \mathbf{z} . Recall that

$$q(\mathbf{z}) = \frac{1}{2} \mathbf{y}^{\top} \left(\mathbb{I}_n + \gamma \sum_{t \in \mathcal{T}} \sum_{i \in \mathcal{N}_t} z_i^t \mathbf{M}_i^t (\mathbf{M}_i^t)^{\top} \right)^{-1} \mathbf{y},$$

where, as previously defined, \mathcal{M} is the $n \times \left(\sum_{t \in \mathcal{T}} |\mathcal{N}_t|\right)$ matrix formed by taking the vectors \mathbf{M}_i^t as its columns. Again, $S = \{i : z_i \neq 0\}$, \mathcal{M}_S is the sub-matrix of \mathcal{M} consisting of the columns indexed by S. Applying (9) we have that:

$$q(\mathbf{z}) = \frac{1}{2} \mathbf{y}^{\top} \bigg(\mathbb{I}_n + \gamma \mathcal{M}_S(\mathcal{M}_S)^{\top} \bigg)^{-1} \mathbf{y}$$

We apply the Woodbury matrix identity (Petersen et al., 2008) to obtain:

$$q(\mathbf{z}) = \frac{1}{2} \left(\mathbf{y}^{\mathsf{T}} \mathbf{y} - \mathbf{y}^{\mathsf{T}} \mathcal{M}_{S} \left(\frac{\mathbb{I}_{|S|}}{\gamma} + \mathcal{M}_{S}^{\mathsf{T}} \mathcal{M}_{S} \right)^{-1} \mathcal{M}_{S}^{\mathsf{T}} \mathbf{y} \right). \tag{10}$$

We can evaluate this expression efficiently by taking the LU decomposition of matrix $(\frac{\mathbb{I}_{|S|}}{\gamma} + \mathcal{M}_S^{\top}\mathcal{M}_S)$.

To compute sub-gradient $\nabla q(\mathbf{z})$, we have that:

$$\frac{\partial q(\mathbf{z})}{\partial z_{i'}^{t'}} = \frac{1}{2} \mathbf{y}^{\top} \frac{\partial}{\partial z_{i'}^{t'}} \left(\left(\mathbb{I}_n + \gamma \sum_{t \in \mathcal{T}} \sum_{i \in \mathcal{N}_t} z_i^t \mathbf{M}_i^t (\mathbf{M}_i^t)^{\top} \right)^{-1} \right) y.$$

We apply the matrix inverse derivative identity (Petersen et al., 2008) and (9) to obtain:

$$\frac{\partial q(\mathbf{z})}{\partial z_{i'}^{t'}} = -\frac{\gamma}{2} \cdot \left((M_{i'}^{t'})^{\top} (\mathbb{I}_n + \gamma \mathcal{M}_S(\mathcal{M}_S)^{\top})^{-1} y \right)^2.$$

Applying the Woodbury matrix identity (Petersen et al., 2008) again yields:

$$\frac{\partial q(\mathbf{z})}{\partial z_{i'}^{t'}} = -\frac{\gamma}{2} \cdot \left((M_{i'}^{t'})^{\top} \cdot \left(\mathbf{y} - \mathcal{M}_S \left(\frac{\mathbb{I}_{|S|}}{\gamma} + \mathcal{M}_S^{\top} \mathcal{M}_S \right)^{-1} \mathcal{M}_S^{\top} \mathbf{y} \right) \right)^2, \quad \forall \ i' \in \mathcal{N}_t, \ t' \in \mathcal{T},$$
(11)

and we can again evaluate this expression efficiently by taking the LU decomposition of matrix $(\frac{\mathbb{I}_{|S|}}{\gamma} + \mathcal{M}_S^{\top} \mathcal{M}_S)$.

C Approximate Algorithm

We present here proofs and additional technical details regarding our approximate algorithm.

C.1 CBCD Algorithm

We show proofs and additional details regarding our efficient block update procedure in our CBCD algorithm.

C.1.1 Proof of Proposition 3

We first prove Problem (6) is an equivalent reformulation of Problem (5); we display the problems below.

Problem (5):

$$\min_{\mathbf{z}^t, w^t} \quad \frac{1}{2} \left\| r - \sum_{i \in \mathcal{N}_t} \mathbf{M}_i^t w_i^t \right\|_2^2 + \frac{1}{2\gamma} \sum_{i \in \mathcal{N}_t} (w_i^t)^2 + \lambda \sum_{i \in \mathcal{N}_t} a_i^t z_i^t$$
s.t.
$$\sum_{j \in \mathcal{C}_i^t} z_j^t \leq |\mathcal{C}_i^t| z_i^t, \quad (1 - z_i^t) w_i^t = 0, \quad z_i^t \in \{0, 1\}, \quad \forall \ i \in \mathcal{N}_t,$$

Problem (6):

$$\min_{\mathbf{z}^{t}} \frac{1}{2} \mathbf{r}^{\mathsf{T}} \left(\mathbb{I}_{n} + \gamma \sum_{i \in \mathcal{N}_{t}} z_{i}^{t} \mathbf{M}_{i}^{t} \left(\mathbf{M}_{i}^{t} \right)^{\mathsf{T}} \right)^{-1} \mathbf{r} + \lambda \sum_{i \in \mathcal{N}_{t}} a_{i}^{t} z_{i}^{t}
\text{s.t.} \quad \sum_{j \in \mathcal{C}_{i}^{t}} z_{j}^{t} \leq |\mathcal{C}_{i}^{t}| z_{i}^{t}, \quad z_{i}^{t} \in \{0, 1\}, \quad \forall \ i \in \mathcal{N}_{t}.$$

Our proof follows closely the proof presented in §B.1. Consider some solution $(\mathbf{z^t})^*$ to

Problem (6) with objective value:

$$\frac{1}{2}\mathbf{r}^{\top} \left(\mathbb{I}_n + \gamma \sum_{i \in \mathcal{N}_t} (z_i^t)^* \mathbf{M}_i^t \left(\mathbf{M}_i^t \right)^{\top} \right)^{-1} \mathbf{r} + \lambda \sum_{i \in \mathcal{N}_t} a_i^t (z_i^t)^*,$$

and note that $(\mathbf{z}^{\mathbf{t}})^*$ satisfies the first and third constraints in Problem (5).

We fix decision vector $\mathbf{z}^{\mathbf{t}}$ to be $(\mathbf{z}^{\mathbf{t}})^*$ in Problem (5) and minimize with respect to w^t . This is given by:

$$\min_{w^{t}} \frac{1}{2} \left\| \mathbf{r} - \sum_{i \in \mathcal{N}_{t}} \mathbf{M}_{i}^{t} w_{i}^{t} \right\|_{2}^{2} + \frac{1}{2\gamma} \sum_{i \in \mathcal{N}_{t}} (w_{i}^{t})^{2} + \lambda \sum_{i \in \mathcal{N}_{t}} a_{i}^{t} (z_{i}^{t})^{*} \qquad (12)$$
s.t.
$$\sum_{j \in \mathcal{C}_{i}^{t}} (z_{i}^{t})^{*} \leq |\mathcal{C}_{i}^{t}| (z_{i}^{t})^{*}, \quad (1 - (z_{i}^{t})^{*}) w_{i}^{t} = 0, \quad (z_{i}^{t})^{*} \in \{0, 1\}, \quad \forall i \in \mathcal{N}_{t},$$

Recall that \mathcal{M}^t is the $n \times |\mathcal{N}_t|$ matrix with columns \mathbf{M}_i^t , $\forall i \in \mathcal{N}_t$, $S = \{i : (z_i^t)^* \neq 0\}$, and \mathcal{M}_S^t is the sub-matrix of \mathcal{M}^t with columns indexed by S. We have that the non-zero coefficient $(w_S^t)^*$ of the optimal solution $(\mathbf{w}^t)^*$ to Problem (12) is given by:

$$(w_S^t)^* = \left(\frac{\mathbb{I}_{|S|}}{\gamma} + (\mathcal{M}_S^t)^\top \mathcal{M}_S^t\right)^{-1} (\mathcal{M}_S^t)^\top \mathbf{y},$$

and that:

$$\mathcal{M}_{S}^{t}(\mathcal{M}_{S}^{t})^{\top} = \sum_{i \in \mathcal{N}_{t}} (z_{i}^{t})^{*} \mathbf{M}_{i}^{t} (\mathbf{M}_{i}^{t})^{\top}.$$
 (13)

Plugging $(\mathbf{w}^{\mathbf{t}})^*$ in to the objective function of (12) and applying the Woodbury matrix identity (Petersen et al., 2008) yields:

$$\begin{split} &\frac{1}{2} \left\| \mathbf{r} - \sum_{i \in \mathcal{N}_t} \mathbf{M}_i^t \left(w_i^t \right)^* \right\|_2^2 + \frac{1}{2\gamma} \sum_{i \in \mathcal{N}_t} ((w_i^t)^*)^2 + \lambda \sum_{i \in \mathcal{N}_t} a_i^t \left(z_i^t \right)^* \\ &= \frac{1}{2} \mathbf{r}^\top \bigg(\mathbb{I}_n + \gamma \sum_{i \in \mathcal{N}_t} (z_i^t)^* \mathbf{M}_i^t \big(\mathbf{M}_i^t \big)^\top \bigg)^{-1} \mathbf{r} + \lambda \sum_{i \in \mathcal{N}_t} a_i^t \left(z_i^t \right)^* \end{split}$$

As such, any solution $(\mathbf{z^t})^*$ to Problem (6) corresponds to solution $((\mathbf{w^t})^*, (\mathbf{z^t})^*)$ to Problem (5), with an identical objective value. The reverse statement is apparent so Problem (6) is an equivalent reformulation of Problem (5).

Next, we show that objective function $\mathbf{z^t} \mapsto q_{\mathbf{r}}(\mathbf{z^t})$ is convex on $\mathbf{z^t} \in [0,1]^{|\mathcal{N}_t|}$. We have that:

$$q_{\mathbf{r}}(\mathbf{z}^{\mathbf{t}}) = \frac{1}{2} \mathbf{r}^{\top} \left(\mathbb{I}_n + \gamma \sum_{i \in \mathcal{N}_t} z_i^t \mathbf{M}_i^t (\mathbf{M}_i^t)^{\top} \right)^{-1} \mathbf{r} + \lambda \sum_{i \in \mathcal{N}_t} a_i^t z_i^t.$$

Note that r is fixed and that matrix $\left(\mathbb{I}_n + \gamma \sum_{i \in \mathcal{N}_t} z_i^t \mathbf{M}_i^t (\mathbf{M}_i^t)^\top\right)$ is positive definite. Using the result from Example 3.4 in Boyd and Vandenberghe (2004) we have that the first term is convex over \mathbf{z} . The second term is linear over \mathbf{z} , so $q_{\mathbf{r}}(\mathbf{z}^t)$ is convex over \mathbf{z} .

C.1.2 Objective and Subgradient Evaluation

We present here a procedure to efficiently evaluate objective $q_{\mathbf{r}}(\mathbf{z}^{\mathbf{t}})$ and subgradient $\nabla q_{\mathbf{r}}(\mathbf{z}^{\mathbf{t}})$, where:

$$q_{\mathbf{r}}(\mathbf{z}^{t}) = \frac{1}{2} \mathbf{r}^{\top} \left(\mathbb{I}_{n} + \gamma \sum_{i \in \mathcal{N}_{t}} z_{i}^{t} \mathbf{M}_{i}^{t} (\mathbf{M}_{i}^{t})^{\top} \right)^{-1} \mathbf{r} + \lambda \sum_{i \in \mathcal{N}_{t}} a_{i}^{t} z_{i}^{t}$$
$$= \frac{1}{2} \mathbf{r}^{\top} \left(\mathbb{I}_{n} + \gamma \mathcal{M}_{S}^{t} (\mathcal{M}_{S}^{t})^{\top} \right)^{-1} \mathbf{r} + \lambda \sum_{i \in \mathcal{N}_{t}} a_{i}^{t} z_{i}^{t}$$

Applying the Woodbury matrix identity (Petersen et al., 2008) yields:

$$q_{\mathbf{r}}(\mathbf{z}^{t}) = \frac{1}{2} \left(\mathbf{r}^{\top} \mathbf{r} - \mathbf{r}^{\top} \mathcal{M}_{S}^{t} \left(\frac{\mathbb{I}_{|S|}}{\gamma} + (\mathcal{M}_{S}^{t})^{\top} \mathcal{M}_{S}^{t} \right)^{-1} (\mathcal{M}_{S}^{t})^{\top} \mathbf{r} \right) + \lambda \sum_{i \in \mathcal{N}_{t}} a_{i}^{t} z_{i}^{t}, \qquad (14)$$

and we can compute this efficiently by taking the LU decomposition of $\left(\frac{\mathbb{I}_{|S|}}{\gamma} + (\mathcal{M}_S^t)^\top \mathcal{M}_S^t\right)$.

For gradient $\nabla q_{\mathbf{r}}(\mathbf{z}^{\mathbf{t}})$ we have that:

$$\frac{\partial q_{\mathbf{r}}(\mathbf{z}^{\mathbf{t}})}{\partial z_{i'}^{t}} = \frac{1}{2} \mathbf{r}^{\top} \frac{\partial}{\partial z_{i'}^{t}} \left(\left(\mathbb{I}_{n} + \gamma \sum_{i \in \mathcal{N}_{t}} z_{i}^{t} \mathbf{M}_{i}^{t} (\mathbf{M}_{i}^{t})^{\top} \right)^{-1} \right) r + \lambda a_{i'}^{t}.$$

We apply the matrix inverse derivative identity and the Woodbury matrix identity (Petersen et al., 2008) to obtain:

$$\frac{\partial q_{\mathbf{r}}(\mathbf{z}^{t})}{\partial z_{i'}^{t}} = -\frac{\gamma}{2} \cdot \left((M_{i'}^{t})^{\top} \cdot \left(\mathbf{r} - \mathcal{M}_{S}^{t} \left(\frac{\mathbb{I}_{|S|}}{\gamma} + (\mathcal{M}_{S}^{t})^{\top} \mathcal{M}_{S}^{t} \right)^{-1} (\mathcal{M}_{S}^{t})^{\top} \mathbf{r} \right) \right)^{2} + \lambda a_{i'}^{t} \quad \forall \ i' \in \mathcal{N}_{t},$$
(15)

which we can compute efficiently by taking the LU decomposition of $\left(\frac{\mathbb{I}_{|S|}}{\gamma} + (\mathcal{M}_S^t)^\top \mathcal{M}_S^t\right)$.

C.1.3 Cutting Plane Recycling

We further discuss here our procedure to recycle cutting planes. We consider two subsequent updates of tree $t \in \mathcal{T}$ in our CBCD procedure. During the first update, say we obtain feasible solution $\mathbf{z}^{\mathbf{t}}$ to Problem (6) and add cutting plane:

$$\nu \ge q_{\mathbf{r}}(\mathbf{z^t}) + \nabla q_{\mathbf{r}}(\mathbf{z^t})(\mathbf{z} - \mathbf{z^t}),$$

where $q_{\mathbf{r}}(\mathbf{z}^{\mathbf{t}})$ is given by (14) and $\nabla q_{\mathbf{r}}(\mathbf{z}^{\mathbf{t}})$ is given by (15). We cache the LU decomposition of: $\left(\frac{\mathbb{I}_{|S|}}{\gamma} + (\mathcal{M}_S^t)^{\top} \mathcal{M}_S^t\right)$ during these evaluations.

Now, consider the second subsequent update of tree $t \in \mathcal{T}$ in our CBCD procedure. The only change to Problem (6) is that residual vector changes to \mathbf{r}' ; solution \mathbf{z}^t is still feasible. We want to add cutting plane:

$$\nu \geq q_{\mathbf{r}'}(\mathbf{z^t}) + \nabla q_{\mathbf{r}'}(\mathbf{z^t})(\mathbf{z} - \mathbf{z^t}),$$

which requires that we evaluate $q_{\mathbf{r}'}(\mathbf{z}^{\mathbf{t}})$ and $\nabla q_{\mathbf{r}'}(\mathbf{z}^{\mathbf{t}})$ using (14) and (15). These evaluations require solving the system:

$$\left(\frac{\mathbb{I}_{|S|}}{\gamma} + (\mathcal{M}_S^t)^{\top} \mathcal{M}_S^t\right) v = (\mathcal{M}_S^t)^{\top} \mathbf{r}',$$

for v, which can be done extremely efficiently since we cache the LU decomposition of $\left(\frac{\mathbb{I}_{|S|}}{\gamma} + (\mathcal{M}_S^t)^\top \mathcal{M}_S^t\right).$

We repeat this cutting plane recycling procedure across all CBCD updates for all solutions $\mathbf{z^t}$ encountered.

D Exploring the Convex Relaxation

As an aside, we discuss a interesting new convex estimator that is of independent interest. Consider this optimization problem:

$$\min_{\mathbf{z}} \quad \frac{1}{2} \mathbf{y}^{\top} \left(\mathbb{I}_n + \gamma \sum_{t \in \mathcal{T}} \sum_{i \in \mathcal{N}_t} z_i^t \mathbf{M}_i^t \left(\mathbf{M}_i^t \right)^{\top} \right)^{-1} \mathbf{y} + \lambda \sum_{t \in \mathcal{T}} \sum_{i \in \mathcal{N}_t} a_i^t z_i^t$$
 (16)

s.t.
$$\sum_{j \in \mathcal{C}_i^t} z_j^t \leq |\mathcal{C}_i^t| z_i^t, \quad \forall \ i \in \mathcal{N}_t, \ t \in \mathcal{T},$$
 (Constraint 16a)

$$z_i^t \in \{0, 1\}, \quad \forall \ i \in \mathcal{N}_t, \ t \in \mathcal{T}.$$
 (Constraint 16b)

We show in §D.1 of the appendix that Problem (16) is a convex integer program and is an equivalent reformulation of Problem (4). Again, note that constraints (16a) and (16b) are separable across trees $t \in \mathcal{T}$.

Convex Relaxation: Consider a convex relaxation of Problem (16), where we relax and replace integrality constraint (16b) with $0 \le z_i^t \le 1$, $\forall i \in \mathcal{N}_t$, $t \in \mathcal{T}$. We can solve the resulting convex, semidefinite program using an efficient tailored algorithm that we present in §D.2 of the appendix. Let ζ_i^t , $\forall i \in \mathcal{N}_t$, $t \in \mathcal{T}$ be the resulting fractional optimal

solution. We find solutions z_i^t , $\forall i \in \mathcal{N}_t$, $t \in \mathcal{T}$ that are feasible for Problem (16) and close to ζ_i^t using the rounding procedure below.

Algorithm 4: Relax and Round Algorithm for Problem (16)

1 solve linear relaxation of Problem (16) for fractional ζ_i^t , $\forall i \in \mathcal{N}_t$, $t \in \mathcal{T}$.

2 for $t \in \mathcal{T}$ do

3 solve ILP (17) for integral solutions z_i^t , $\forall i \in \mathcal{N}_t$

4 end

5 return z

Rounding Procedure fo Feasible Solutions Let solutions z_i^t represent which elements of ζ_i^t to round to 1, for all $i \in \mathcal{N}_t$, $t \in \mathcal{T}$. Note that constraint (16a) separates across trees $t \in \mathcal{T}$. For each tree t, we want to round the largest elements of ζ_i^t , $\forall i \in \mathcal{N}_t$ to 1, such that constraint (16a) is satisfied. We do so by solving the following integer linear program:

$$\sum_{i \in \mathcal{N}_t} \max_{z_i^t} \quad \zeta_i^t z_i^t, \quad \text{s.t.} \quad \sum_{j \in \mathcal{C}_i^t} z_j^t \leq |\mathcal{C}_i^t| z_i^t, \quad z_i^t \in \{0, 1\}, \quad \forall \ i \in \mathcal{N}_t.$$
 (17)

We repeat this rounding procedure for all trees $t \in \mathcal{T}$ to obtain our final feasible solution to Problem (16). We present our full relax and round procedure in Algorithm 4, which returns integral solutions z_i^t , $\forall i \in \mathcal{N}_t$, $t \in \mathcal{T}$ feasible for Problem (16).

Solving on ILP (17): We exploit problem structure in order to solve ILP (17) efficiently. In the proposition below, we establish two important properties of the problem.

Proposition 4. ILP (17) is a knapsack problem with conflict graph G = (V,E) where $V = \mathcal{N}_t$ and $E = \{(i,j) \ \forall \ i \in \mathcal{N}_t, \ j \in \mathcal{C}_i^t\}$. Conflict graph G is chordal.

We prove this proposition in §D.3 of the appendix. As a result of Proposition 4, we can apply ALGCH from Pferschy and Schauer (2009) to solve Problem (17) to optimality in pseudo-polynomial time. We can also use the associated polynomial-time approximation scheme to find good solutions efficiently.

Discussion: Our relax-and-round procedure has either a pseudo-polynomial or polynomial

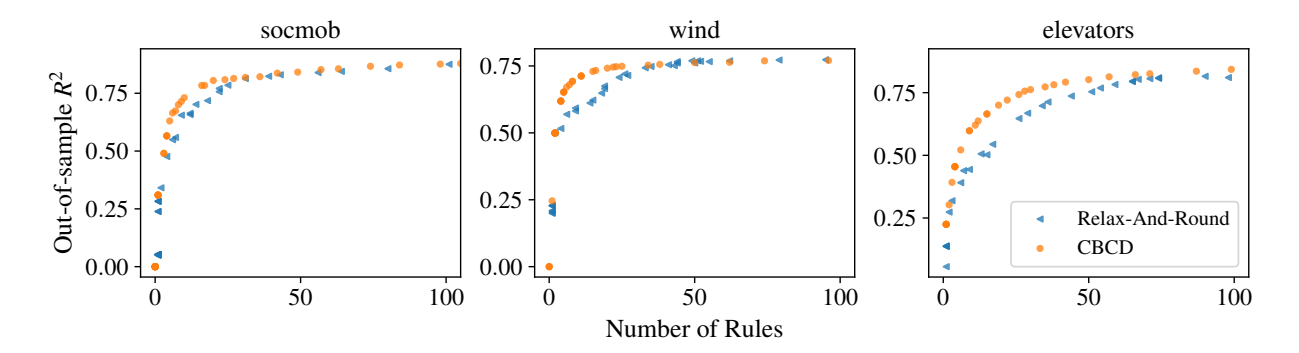


Figure 13: Comparison of regularization paths obtained by our relax-and-round algorithm and CBCD. CBCD typically obtains higher quality solutions compared to relax-and-round.

time complexity, depending on the rounding method used. However, we note that the solutions obtained through the relax-and-round procedure are typically of lower quality than those produced by our CBCD approximate algorithm. In Figure 13, we compare the performance of relax-and-round and CBCD by computing regularization paths on three examples: ensembles of 500 depth-7 trees trained on the SOCMOB, WIND, and ELEVATORS datasets from the OpenML benchmark repository Bischl et al. (2017). From these plots, we observe that our CBCD approximate algorithm noticeably outperforms relax-and-round in terms of predictive accuracy.

D.1 Problem Reformulation

We show here that Problem (16) is an equivalent CIP reformulation of Problem (4). We display both of these problems below.

Problem (4):

$$\min_{z_i^t, w_i^t} \quad \frac{1}{2} \left\| \mathbf{y} - \sum_{t \in \mathcal{T}} \sum_{i \in \mathcal{N}_t} \mathbf{M}_i^t w_i^t \right\|_2^2 + \frac{1}{2\gamma} \sum_{t \in \mathcal{T}} \sum_{i \in \mathcal{N}_t} (w_i^t)^2 + \lambda \sum_{t \in \mathcal{T}} \sum_{i \in \mathcal{N}_t} a_i^t z_i^t \\
\text{s.t.} \quad \sum_{j \in \mathcal{C}_i^t} z_j^t \leq |\mathcal{C}_i^t| z_i^t, \quad \forall \ i \in \mathcal{N}_t, \ t \in \mathcal{T} \\
(1 - z_i^t) \ w_i^t = 0, \quad \forall \ i \in \mathcal{N}_t, \ t \in \mathcal{T} \\
z_i^t \in \{0, 1\}, \quad \forall \ i \in \mathcal{N}_t, \ t \in \mathcal{T},$$

Problem (16):

$$\min_{\mathbf{z}} \quad \frac{1}{2} \mathbf{y}^{\top} \left(\mathbb{I}_{n} + \gamma \sum_{t \in \mathcal{T}} \sum_{i \in \mathcal{N}_{t}} z_{i}^{t} \mathbf{M}_{i}^{t} \left(\mathbf{M}_{i}^{t} \right)^{\top} \right)^{-1} \mathbf{y} + \lambda \sum_{t \in \mathcal{T}} \sum_{i \in \mathcal{N}_{t}} a_{i}^{t} z_{i}^{t}
\text{s.t.} \quad \sum_{j \in \mathcal{C}_{i}^{t}} z_{j}^{t} \leq |\mathcal{C}_{i}^{t}| z_{i}^{t}, \quad \forall \ i \in \mathcal{N}_{t}, \ t \in \mathcal{T},
z_{i}^{t} \in \{0, 1\}, \quad \forall \ i \in \mathcal{N}_{t}, \ t \in \mathcal{T}.$$

The proof that (16) is an equivalent reformulation of (4) follows directly from the proof of Proposition 1, presented in §B.1.1.

The objective of IP (16):

$$\frac{1}{2}\mathbf{y}^{\top} \left(\mathbb{I}_n + \gamma \sum_{t \in \mathcal{T}} \sum_{i \in \mathcal{N}_t} z_i^t \mathbf{M}_i^t \left(\mathbf{M}_i^t \right)^{\top} \right)^{-1} \mathbf{y} + \lambda \sum_{t \in \mathcal{T}} \sum_{i \in \mathcal{N}_t} a_i^t z_i^t,$$

is again convex over \mathbf{z} since $\left(\mathbb{I}_n + \gamma \sum_{i \in \mathcal{N}_t} z_i^t \mathbf{M}_i^t (\mathbf{M}_i^t)^\top\right)$ is positive definite. Using the result from Example 3.4 (Boyd and Vandenberghe, 2004) yields that convex compositions of affine functions are convex.

D.2 Linear Relaxation Algorithm

We consider this linear relaxation to Problem (16):

$$\min_{\mathbf{z}} \quad q_{LR}(\mathbf{z}) = \frac{1}{2} \mathbf{y}^{\top} \left(\mathbb{I}_n + \gamma \sum_{t \in \mathcal{T}} \sum_{i \in \mathcal{N}_t} z_i^t \mathbf{M}_i^t \left(\mathbf{M}_i^t \right)^{\top} \right)^{-1} \mathbf{y} + \lambda \sum_{t \in \mathcal{T}} \sum_{i \in \mathcal{N}_t} a_i^t z_i^t \qquad (18)$$
s.t.
$$\sum_{j \in \mathcal{C}_i^t} z_j^t \leq |\mathcal{C}_i^t| z_i^t, \quad \forall \ i \in \mathcal{N}_t, \ t \in \mathcal{T},$$

$$z_i^t \in [0, 1], \quad \forall \ i \in \mathcal{N}_t, \ t \in \mathcal{T}.$$

We present a specialized outer approximation algorithm to solve Problem (18) efficiently. Objective $q_{LR}(\mathbf{z})$ is convex and sub-differentiable; for all $\mathbf{z}' \in [0, 1]^m$ we have that: $q_{LR}(\mathbf{z}') \geq q_{LR}(\mathbf{z}) + \nabla q_{LR}(\mathbf{z})^{\top}(\mathbf{z}' - \mathbf{z})$. Given a sequence of feasible solutions $\mathbf{z}^{(0)}, z^{(1)}, \dots \mathbf{z}^{(h)}$ for Problem (18), we have that:

$$\max_{k=0\dots h} q_{LR}(\mathbf{z}^{(k)}) + \nabla q_{LR}(\mathbf{z}^{(k)})(\mathbf{z} - \mathbf{z}^{(k)}) \leq q_{LR}(\mathbf{z}).$$

.

In iteration h of our outer approximation algorithm, we solve LP:

$$\min_{z,\nu} \quad \nu$$
s.t.
$$\sum_{j \in \mathcal{C}_i^t} z_j^t \leq |\mathcal{C}_i^t| z_i^t, \quad z_i^t \in [0,1], \quad \forall i \in \mathcal{N}_t, \ t \in \mathcal{T},$$

$$\nu \geq q_{LR}(\mathbf{z}^{(\mathbf{k})}) + \nabla q_{LR}(\mathbf{z}^{(\mathbf{k})})^\top (\mathbf{z} - \mathbf{z}^{(\mathbf{k})}) \quad \forall k \in \{0,1,\ldots,h\},$$

where ν is a lower bound for the optimal objective value $q_{LR}(\mathbf{z}^*)$, to obtain $\mathbf{z}^{(\mathbf{h}+\mathbf{1})}$ and $\nu^{(h+1)}$. We terminate our algorithm when $q_{LR}(\mathbf{z}^{(\mathbf{h})})$ is equal to $\nu^{(h)}$; our algorithm terminates in a finite number of iterations since the feasible for \mathbf{z} is compact and returns optimal solution \mathbf{z}^* to Problem (18).

D.3 Proof of Proposition (4)

We first prove that ILP (17) is a knapsack problem with conflict graph G = (V, E) where $V = \mathcal{N}_t$ and $E = \{(i, j) \ \forall \ i \in \mathcal{N}_t, \ j \in \mathcal{C}_i^t\}$. Consider the these two optimization problems. **Problem** (17)

$$\sum_{i \in \mathcal{N}_t} \max_{z_i^t} \quad \zeta_i^t z_i^t,$$
s.t.
$$\sum_{j \in \mathcal{C}_i^t} z_j^t \leq |\mathcal{C}_i^t| z_i^t, \quad \forall \ i \in \mathcal{N}_t,$$

$$z_i^t \in \{0, 1\}, \quad \forall \ i \in \mathcal{N}_t.$$

Knapsack Conflict Graph (KCG)

$$\sum_{i \in \mathcal{N}_t} \max_{z_i^t} \quad \zeta_i^t z_i^t,$$
 s.t. $z_i^t + z_j^t \le 1$, $\forall (i, j) \in \{(i, j) \ \forall \ i \in \mathcal{N}_t, \ j \in \mathcal{C}_i^t\}$
$$z_i^t \in \{0, 1\}, \quad \forall \ i \in \mathcal{N}_t.$$

and Schauer (2009). Any feasible solution to Problem (17) is feasible for (KCG), and vice versa, as the first constraint in both problems is equivalent. The objective functions of both problems are equivalent, so (KCG) is an equivalent reformulation of Problem (17). Next, consider conflict graph G = (V, E) where $V = \mathcal{N}_t$ and $E = \{(i, j) \ \forall \ i \in \mathcal{N}_t, \ j \in \mathcal{C}_i^t\}$. The edges in set E connect every node $i \in \mathcal{N}_t$ with all of its descendant nodes $j \in \mathcal{C}_i^t$, so graph G is a transitive closure of a tree which is chordal.

Problem KCG is the ILP form of a knapsack conflict graph problem shown in Pferschy

E Proofs of the Theoretical Results in Section 4

Given a function $f : \mathbb{R}^p \to \mathbb{R}$, we define $\mathbf{f} = (f(\mathbf{x}_1), ..., f(\mathbf{x}_n))^\top$; we define vectors such as \mathbf{f}^* and $\hat{\mathbf{f}}$ by analogy. We also let $\mathbf{y} = (y_1, ..., y_n)^\top$ and $\boldsymbol{\epsilon} = (\epsilon_1, ..., \epsilon_n)^\top$. We use $\|\cdot\|$ to denote the Euclidean norm. As before, we use \mathbf{x} to denote vectors in \mathbb{R}^p and write x_j for the j-th coordinate of \mathbf{x} .

Consider an arbitrary positive integer s. In our analysis, we replace random functional classes $C_k(s)$ with larger deterministic classes $\mathcal{F}_k(s)$ for each $k \in \{1, 2, 3\}$. More specifically, we let $\mathcal{F}_k(s)$ consist of all possible functions that might appear in $C_k(s)$. For example, we define $\mathcal{F}_1(s)$ as the class of all functions $f: \mathbb{R}^p \to \mathbb{R}$ of the form $f(\mathbf{x}) = \sum_{t=1}^s \beta_t \Pi_{l=1}^{d_t} I_{lt}(\mathbf{x})$, where $d_t \in \{1, ..., D\}$, β_t are real-valued coefficients, and I_{lt} are indicator functions of the form $I_{lt}(\mathbf{x}) = \mathbf{1}_{\{x_j \leq s_{lt}\}}$ or $I_{lt}(\mathbf{x}) = \mathbf{1}_{\{x_j > s_{lt}\}}$ for some $j \in \{1, ..., p\}$ and real-valued split-points s_{lt} .

We define $\mathcal{F}_2(s)$ as a subset of $\mathcal{F}_1(s)$ by imposing an additional attribute constraint: $\sum_{t=1}^{s} d_t \mathbf{1}_{\{\beta_t \neq 0\}} \leq s$. Similarly, we define $\mathcal{F}_3(s)$ as a subset of $\mathcal{F}_1(s)$ by requiring $\sum_{t=1}^{s} v_t \mathbf{1}_{\{\beta_t \neq 0\}} \leq s$, where v_t is the number of distinct features j that appear in the term $\prod_{l=1}^{d_t} I_{lt}(\mathbf{x})$. Consequently, $\mathcal{C}_k(K) \subseteq \mathcal{F}_k(K)$ for each training sample and each $k \in \{1, 2, 3\}$.

We will use the following result, which is derived in Appendix E.4.

Lemma 1. Each of the following inequalities,

(i)
$$\sup_{f \in \mathcal{F}_1(2K)} \boldsymbol{\epsilon}^{\top} \mathbf{f} \lesssim \sigma \sqrt{KD \log(enp) + \log(1/\delta_0)} \|f\|$$

(ii)
$$\sup_{f \in \mathcal{F}_2(2K)} \boldsymbol{\epsilon}^{\top} \mathbf{f} \lesssim \sigma \sqrt{K \log(enp) + \log(1/\delta_0)} \|f\|$$

(iii)
$$\sup_{f \in \mathcal{F}_3(2K)} \boldsymbol{\epsilon}^{\top} \mathbf{f} \lesssim \sigma \sqrt{K \log(enp) + \log(1/\delta_0)} \|f\|,$$

holds with probability at least $1 - \delta_0$.

E.1 Proof of Theorem 1

We first establish the result for \widehat{f}_1 . Let $r_1 = KD\log(enp)/n$ and note that this definition matches the one from Corollary 1. Consider an arbitrary $f \in \mathcal{C}_1(K)$ and note that

$$\|\mathbf{y} - \widehat{\mathbf{f}}_1\|^2 + \frac{1}{\gamma} \|w(f)\| \le \|\mathbf{y} - \mathbf{f}\|^2 + \frac{1}{\gamma} \|w(f)\|^2$$

which implies

$$\|\mathbf{f}^* - \widehat{\mathbf{f}}_1\|^2 \le \|\mathbf{f}^* - \mathbf{f}\|^2 + 2\boldsymbol{\epsilon}^\top (\widehat{\mathbf{f}}_1 - \mathbf{f}) + \frac{1}{\gamma} \|w(f)\|^2.$$
 (20)

Note that, for each training sample, $\widehat{f}_1 - f \in \mathcal{F}_1(2K)$. Consequently, by Lemma 1, we have

$$\boldsymbol{\epsilon}^{\top}(\widehat{\mathbf{f}}_1 - \mathbf{f}) \lesssim \sigma \sqrt{nr_1 + \log(1/\delta_0)} \|\widehat{\mathbf{f}}_1 - \mathbf{f}\|$$
 (21)

with probability at least $1 - \delta_0$. We conduct the rest of the argument on the event where inequality (21) holds. Combining inequalities (21) with (20), we derive, for some universal constant c,

$$\|\mathbf{f}^* - \widehat{\mathbf{f}}_1\|^2 \leq \|\mathbf{f}^* - \mathbf{f}\|^2 + c\sigma\sqrt{nr_1 + \log(1/\delta_0)}\|\widehat{\mathbf{f}}_1 - \mathbf{f}\| + \frac{1}{\gamma}\|w(f)\|^2$$

$$\leq \|\mathbf{f}^* - \mathbf{f}\|^2 + c\sigma\sqrt{nr_1 + \log(1/\delta_0)}(\|\mathbf{f}^* - \widehat{\mathbf{f}}_1\| + \|\mathbf{f}^* - \mathbf{f}\|) + \frac{1}{\gamma}\|w(f)\|^2. (22)$$

We bound the second and third terms on the right-hand side of the last inequality by applying inequality

$$2ab \le qa^2 + q^{-1}b^2, (23)$$

which holds for every q > 0 and $a, b \in \mathbb{R}$. Setting q = 2, we derive bounds

$$c\sigma\sqrt{nr_1+\log(1/\delta_0)}\|\mathbf{f}^*-\widehat{\mathbf{f}}_1\| \le 2c\sigma^2\left[nr_1+\log(1/\delta_0)\right] + \|\mathbf{f}^*-\widehat{\mathbf{f}}_1\|^2/2$$

and

$$c\sigma\sqrt{nr_1+\log(1/\delta_0)}\|\mathbf{f}^*-\mathbf{f}\| \lesssim \sigma^2[nr_1+\log(1/\delta_0)]+\|\mathbf{f}^*-\mathbf{f}\|^2.$$

Combining these bounds with inequality 22, we derive

$$\|\mathbf{f}^* - \widehat{\mathbf{f}}_1\|^2 \lesssim \|\mathbf{f}^* - \mathbf{f}\|^2 + \sigma^2 [nr_1 + \log(1/\delta_0)] + \frac{1}{\gamma} \|w(f)\|^2$$

which implies

$$||f^* - \widehat{f_1}||_n^2 \lesssim ||f - f^*||_n^2 + \sigma^2 [r_1 - \log(\delta_0)/n] + \frac{1}{n\gamma} ||w(f)||^2.$$

Thus, we have established the bound in the first claim of Theorem 1. The corresponding bounds for \hat{f}_2 and \hat{f}_3 follow by (nearly) identical arguments, which only require recalling the definitions of r_2 and r_3 from Corollary 1, as well as replacing subscript "1" with "2" or "3", respectively.

E.2 Proof of Corollary 1

We fix an arbitrary $k \in \{1, 2, 3\}$ and define $\tilde{\mathcal{C}}_k(K) = \{f \in \mathcal{C}_k(K), \text{ s.t. } ||w(f)||_{\infty} \leq c\}$. It follows from Theorem 1 that inequality

$$\|\widehat{f}_k - f^*\|_n^2 \lesssim \inf_{f \in \widetilde{\mathcal{C}}_k(K)} \left\{ \|f_k - f^*\|_n^2 + \frac{1}{n\gamma} \|w(f)\|^2 \right\} + \sigma^2 \left[r_k - \log(\delta_0)/n \right]$$
 (24)

holds with probability at least $1 - \delta_0$. Note that $||w(f)||_{\infty} \leq c$ implies $||w(f)||^2 \leq c^2 K$, and hence $\frac{1}{n\gamma}||w(f)||^2 \lesssim \sigma^2 r_k$ because of the assumption $\gamma \gtrsim K(\sigma^2 n r_k)^{-1}$. Consequently, taking into account the assumption on $\inf_{f \in \tilde{\mathcal{C}}_k(K)} ||f_k - f^*||_n^2$, we can re-write inequality (24) as follows:

$$\|\widehat{f}_k - f^*\|_n^2 \lesssim \sigma^2 [r_k - \log(\delta_0)/n].$$

We note that $\log(1/\delta_k) = nr_k$. Thus, taking $\delta_0 = \delta_k$, we conclude that $\|\widehat{f}_k - f^*\|_n^2 \lesssim \sigma^2 r_k$ with probability at least $1 - \delta_k$.

E.3 Proof of Corollary 2

By the assumptions of Corollary 2, there exists a (data-dependent) function $f_k \in \mathcal{C}_k(K)$, such that

$$\|\mathbf{f}_k - \mathbf{f}^*\|^2 \lesssim \sigma^2 n r_k \quad \text{and} \quad \|w(f_k)\|^2 \lesssim K$$
 (25)

with probability at least $1 - \epsilon$. To simplify the presentation, we define $G(f) = \|\mathbf{y} - \mathbf{f}\|^2 + \frac{1}{\gamma} \|w(f)\|$. Because $UB = G(\widetilde{f}_k)$, $LB \leq G(f_k)$, and $UB = LB/(1 - \tau)$, we derive

$$G(\widetilde{f_k}) \le G(f_k)/(1-\tau),$$

and hence

$$\|\mathbf{y} - \widetilde{\mathbf{f}}_k\|^2 \le \|\mathbf{y} - \mathbf{f}_k\|^2 / (1 - \tau) + \frac{1}{\gamma} \|w(f_k)\|^2 / (1 - \tau).$$

Consequently,

$$\|\mathbf{f}^* - \widetilde{\mathbf{f}}_k\|^2 \le \|\mathbf{f}^* - \mathbf{f}_k\|^2 + 2\epsilon^{\top}(\widetilde{\mathbf{f}}_k - \mathbf{f}_k) + 2\tau \|\mathbf{f}^* - \mathbf{f}_k\|^2 + 2\tau \|\epsilon\|^2 + \frac{1}{\gamma} \|w(f_k)\|^2 / (1 - \tau),$$

which is a slightly modified version of inequality (20) in the proof of Theorem 1. Note that $\tilde{\mathbf{f}}_k \in \mathcal{C}_k(K)$ and $1/(1-\tau) \lesssim 1$. Repeating the steps in the proof of Theorem 1, while accounting for the new terms, we conclude that inequality

$$\|\widetilde{\mathbf{f}}_k - \mathbf{f}^*\|^2 \lesssim \|\mathbf{f}_k - \mathbf{f}^*\|^2 + \sigma^2 [nr_k + \log(1/\delta_0)] + \frac{1}{\gamma} \|w(f_k)\|^2 + \tau \|\epsilon\|^2$$

holds with probability at least $1 - \delta_0$. Letting $\gamma \gtrsim K(\sigma^2 n r_k)^{-1}$, taking into account (25), and setting $\delta_0 = \delta_k/2$, we derive inequality

$$\|\widetilde{\mathbf{f}}_k - \mathbf{f}^*\|^2 \lesssim \sigma^2 n r_k + \|\boldsymbol{\epsilon}\|^2 \tau, \tag{26}$$

which holds with probability at least $1 - \delta_k/2 - \epsilon$.

Standard chi-square tail bounds (for example, those in Section 8.3.2 of Bühlmann and Van De Geer, 2011) imply that, with an appropriate multiplicative constant, inequality $\|\boldsymbol{\epsilon}\|^2 \lesssim \sigma^2 n(1+r_k)$ holds with probability at least $1-\delta_k/2$. Thus, after dividing by n, we can re-write inequality (26) as

$$\|\widetilde{f}_k - f^*\|_n^2 \lesssim \sigma^2 r_k + \sigma^2 \tau,$$

which holds with probability at least $1 - \delta_k - \epsilon$.

E.4 Proof of Lemma 1

Recall that functions in the class $\mathcal{F}_1(2K)$ have the form $f(\mathbf{x}) = \sum_{t=1}^{2K} \beta_t \prod_{l=1}^{d_t} I_{lt}(\mathbf{x})$, where each indicator I_{lt} determines a split. We define $h_t = \prod_{l=1}^{d_t} I_{lt}$ and, as before, we let $\mathbf{h}_t = (h_t(\mathbf{x}_1), ..., h_t(\mathbf{x}_n))^{\top}$. Note that $\mathbf{f} = \sum_{t=1}^{2K} \beta_t \mathbf{h}_t$.

We start by fixing the collection $\{\mathbf{h}_1,...,\mathbf{h}_{2K}\}$, while allowing coefficients β_t to vary, and uniformly bounding the corresponding inner products $\boldsymbol{\epsilon}^{\top}\mathbf{f}$. We choose an orthonormal basis $\boldsymbol{\Psi} = [\boldsymbol{\psi}_1,...,\boldsymbol{\psi}_{2K}]$, such that the corresponding linear space contains the space spanned by the vectors $\mathbf{h}_1,...,\mathbf{h}_{2K}$. First, observe that

$$\boldsymbol{\epsilon}^{\top}\mathbf{f} \leq \|\boldsymbol{\Psi}^{\top}\boldsymbol{\epsilon}\|\|\mathbf{f}\|$$

for every choice of coefficients $\beta_1,...,\beta_{2K}$. Next, note that $\|\mathbf{\Psi}^{\top}\boldsymbol{\epsilon}\|^2/\sigma^2$ has chi-square dis-

tribution with at most 2K degrees of freedom. Using a chi-square tail bound (for example, the one in Section 8.3.2 of Bühlmann and Van De Geer, 2011), we derive that $\|\mathbf{\Psi}^{\top}\boldsymbol{\epsilon}\|^2 \lesssim \sigma^2 K(1+a)$ with probability at least $1 - \exp(-4Ka)$. Putting everything together, we conclude that, with probability at least $1 - \exp(-4Ka)$, inequality

$$\epsilon^T \mathbf{f} \lesssim \left[\sigma^2 K(1+a) \right]^{1/2} \|\mathbf{f}\|$$
(27)

holds uniformly for all $\beta_1, ..., \beta_{2K}$.

We now extend this bound so that it holds for all collections $\{\mathbf{h}_t\}_{t=1}^{2K}$ allowed by the corresponding functional class, i.e., $\mathcal{F}_1(2K)$, $\mathcal{F}_2(2K)$, or $\mathcal{F}_3(2K)$.

Class $\mathcal{F}_1(2K)$ and claim (i) of Lemma 1. Consider all the possible values that vectors \mathbf{h}_t can take. For each \mathbf{h}_t , the underlying indicator function h_t corresponds to at most D splits, each involving one of the p features. Because \mathbf{h}_t evaluates h_t at the training data that has n observations, we only need to consider n possible locations for each split point; there are also two options for the direction of each split inequality. Consequently, there are at most $(2np)^D$ values that vectors \mathbf{h}_t can take, and hence the number of distinct sets $\{\mathbf{h}_t\}_{t=1}^{2K}$ is bounded by $(2np)^{2KD}$. Applying the union bound over all such sets, we deduce that (27) holds uniformly over all $f \in \mathcal{F}_1(2K)$ with probability at least $1 - \exp(-4Ka + 2KD\log(2np))$. Taking $a = D\log(2np)/2 + \log(1/\delta_0)/(4K)$, we conclude that inequality

$$\sup_{f \in \mathcal{F}_1(2K)} \boldsymbol{\epsilon}^T \mathbf{f} \lesssim \left[\sigma^2 K D \log(enp) + \sigma^2 \log(1/\delta_0) \right]^{1/2} \|\mathbf{f}\|$$

holds with probability at least $1 - \delta_0$.

Class $\mathcal{F}_2(2K)$ and claim (ii) of Lemma 1. Functions in the class $\mathcal{F}_2(2K)$ have the form $f(\mathbf{x}) = \sum_{t=1}^s \beta_t \prod_{l=1}^{d_t} I_{lt}(\mathbf{x})$, where each indicator I_{lt} determines a split, $s \in \{1, ..., 2K\}$ is the number of rules, and the sum of the rule-depths is at most 2K. We will suppose that the sum is exactly 2K, as we can achieve this by repeating some of the splits.

Let N_{2K} denote the number of ways we can distribute the total depth 2K among the rules associated with function f. We note that during this distribution process we also specify the *number* of rules for f, which is allowed to be between one and 2K. Our distribution problem is equivalent to counting the number of ways we can distribute 2K balls into L buckets, where $1 \le L \le 2K$, and the balls are indistinguishable. Given an L, we can upper-bound the count by the number of ways we can place L-1 separators in 2K-1 locations. Hence,

$$N_{2K} \le \sum_{k=0}^{2K-1} {2K-1 \choose k} = 2^{2K-1}.$$

Note that the total number of splits in the rules equals the total depth, which is 2K. Once we have decided on the number of rules and distributed the depths among the rules, we just need to consider all the possible ways of making 2K splits. Arguing as before, we bound the number of ways by $(2np)^{2K}$.

Putting everything together, we can bound the number of distinct sets $\{\mathbf{h}_t\}_{t=1}^{2K}$ by $2^{2K-1}(2np)^{2K}$. Applying the union bound over all such sets, we deduce that (27) holds uniformly over all $f \in \mathcal{F}_2(2K)$ with probability at least $1 - \exp(-4Ka + 2K\log(4enp))$. Taking $a = \log(4enp)/2 + \log(1/\delta_0)/(4K)$, we conclude that inequality

$$\sup_{f \in \mathcal{F}_2(2K)} \boldsymbol{\epsilon}^T \mathbf{f} \lesssim \left[\sigma^2 K \log(enp) + \sigma^2 \log(1/\delta_0) \right]^{1/2} \|\mathbf{f}\|$$

holds with probability at least $1 - \delta_0$.

Class $\mathcal{F}_3(2K)$ and claim (iii) of Lemma 1. Relative to the case with the class $\mathcal{F}_1(2K)$ we have the additional restriction that the sum over the rules of the numbers of distinct features per rule is at most 2K. The number of ways to chose the features used in the rules is bounded by p^{2K} . Arguing as we did for claim (ii), we note that the number of ways to distribute these chosen 2K features across the rules is bounded by 2^{2K-1} . Note that a

given feature in a given rule can be used in at most two splits, otherwise we can discard some of the splits. Hence, given the allocation of the 2K features across the rules, we need to consider at most 4K splits, each with at most n possible split-point locations and two directions for the split inequality. This leads to at most $(2n)^{4K}$ possibilities.

Putting everything together, we can bound the number of distinct sets $\{\mathbf{h}_t\}_{t=1}^{2K}$ by $p^{2K}2^{2K-1}(2n)^{4K}$. Applying the union bound over all such sets, we deduce that (27) holds uniformly over all $f \in \mathcal{F}_2(2K)$ with probability at least $1 - \exp(-4Ka + 4K\log(2enp))$. Taking $a = \log(2enp) + \log(1/\delta_0)/(4K)$, we conclude that inequality

$$\sup_{f \in \mathcal{F}_3(2K)} \boldsymbol{\epsilon}^T \mathbf{f} \lesssim \left[\sigma^2 K \log(enp) + \sigma^2 \log(1/\delta_0) \right]^{1/2} \|\mathbf{f}\|$$

holds with probability at least $1 - \delta_0$.

F Experiments

We present additional details regarding the experimental evaluation of our framework.

F.1 Datasets

Name	Observations	Features
autoMpg	398	25
ESL	488	4
no2	500	7
stock	950	9
socmob	1156	39
Moneyball	1232	72
us_crime	1994	1954
space_ga	3107	6
pollen	3848	4
abalone	4177	10
Mercedes_Benz_Greener_Manufacturing	4209	563
mtp	4450	202
satellite_image	6435	36
$wine_quality$	6497	11
wind	6574	14
cpu_small	8192	12
bank32nh	8192	32
kin8nm	8192	8
puma32H	8192	32
Ailerons	13750	40
pol	15000	48
elevators	16599	18
houses	20640	8
house_16H	22784	16
mv	40768	14

Table 3: Datasets considered in our experimental evaluation